New Mexico GEOLOGY

Spring, 2018
Volume 40, Number 1

New Mexico Bureau of Geology and Mineral Resources/A Division of New Mexico Tech

New Mexico GEOLOGY

Spring, 2018
Volume 40, Number 1

Cover Image

The Aden shield and crater rim, located 40 km southwest of Las Cruces, New Mexico, lies within the Organ Mountains-Desert Peaks National Monument administered by the Bureau of Land Management. Aden is situated along the northeastern side of the Potrillo Volcanic Field, which covers 1,000 square kilometers and is represented by numerous eruptive centers and associated lava fields that were active during the Late Quaternary. The lava flows at Aden resulted from the extrusion of relatively low-viscosity basaltic magmas that spread passively across the landscape similar to present-day eruptions on Hawaii. Successive eruptions created a shield volcano with a well-preserved, central crater. Aden Crater exhibits a rugged, circular rim consisting of solidified spatter, and contained a molten lake of lava when the volcano was last active. Volcanic features of the Potrillo Volcanic Field also include maars, including the extensively studied Kilbourne Hole, which result when rising magma encounters groundwater, resulting in a violent eruption of steam, country rock, and magma into the atmosphere. Description and interpretation of features of the Aden basalt field are discussed in the paper beginning on page 17 of this issue. *Photograph and caption courtesy of René De Hon.*

A publication of the
New Mexico Bureau of Geology and Mineral Resources,
a division of the New Mexico Institute of Mining and Technology

Science and Service
ISSN 0196-948X

New Mexico Bureau of Geology and Mineral Resources
Director and State Geologist
Dr. Nelia W. Dunbar

Geologic Editor: Bruce Allen
Layout and Production Editor: Richard Arthur
Managing Editor: Gina D'Ambrosio

Cartography & Graphics: Leo Gabaldon

New Mexico Geology is an online publication available as a free PDF download from the New Mexico Bureau of Geology and Mineral Resources website. Subscribe to receive e-mail notices when each issue is available at: geoinfo.nmt.edu/publications/subscribe.

Editorial Matter: Articles submitted for publication should follow the guidelines at: <geoinfo.nmt.edu/publications/periodicals/nmg/NMGguidelines.html>. Address inquiries to Bruce Allen, Geologic Editor, New Mexico Bureau of Geology and Mineral Resources, 801 Leroy Place, Socorro, NM 87801. For telephone inquiries call (575) 835-5177 or use the email address given below.

Email: NMBG-NMGeology@nmt.edu

geoinfo.nmt.edu/publications/periodicals/nmg

Baculites (Ammonoidea) and the age of the Pierre Shale in the eastern Raton Basin, south-central Colorado

Keith Berry[1]
[1]Science Department, Hoehne Re-3 School District, Hoehne, CO 81046; *keith.berry@hoehnesd.org*

Abstract

The Pierre Shale is a marine deposit that accumulated in the Cretaceous Western Interior Seaway during the onset of Laramide tectonism in the southern Rocky Mountains region. In the eastern part of the Raton Basin near Trinidad, Colorado, ammonite biostratigraphy suggests that the base of the Pierre Shale lies within or slightly above the Lower Campanian *Scaphites hippocrepis III* ammonite range zone (81.8–80.5 Ma), and the top of the Pierre Shale corresponds with the Lower Maastrichtian *Baculites clinolobatus* Zone (69.59 + 0.36 Ma). These data are consistent with previous estimates for the age of the base of the Pierre Shale in the Raton Basin, and indicate that the top of the Pierre Shale (base of the overlying Trinidad Sandstone) in the eastern part of the basin lies near the Lower-Upper Maastrichtian substage boundary. A Late Maastrichtian age for the Trinidad Sandstone near Trinidad has a bearing on the timing of geological events associated with the eastward retreat of the Western Interior Seaway from the region during the Late Cretaceous.

Introduction

The Pierre Shale was deposited within the Western Interior Seaway during an early phase of Laramide tectonism, which resulted in areas of regional subsidence and uplift associated with subduction of the Farallon tectonic plate beneath western North America (Baltz, 1965; Cather, 2004; Slattery et al., 2015; Heller and Liu, 2016). In the Raton Basin of northeastern New Mexico and south-central Colorado (Fig.1), the Pierre Shale is underlain by the Niobrara Formation and overlain by the Trinidad Sandstone (Lee, 1917). The age of the base of the Pierre Shale is constrained by ammonite biostratigraphy of the uppermost part of the Niobrara Formation in the Raton Basin and surrounding regions (Scott et al., 1986; Molenaar et al., 2002; Merewether et al., 2011). The age of the top of the Pierre Shale is similarly constrained by ammonite biostratigraphy of the upper part of the formation.

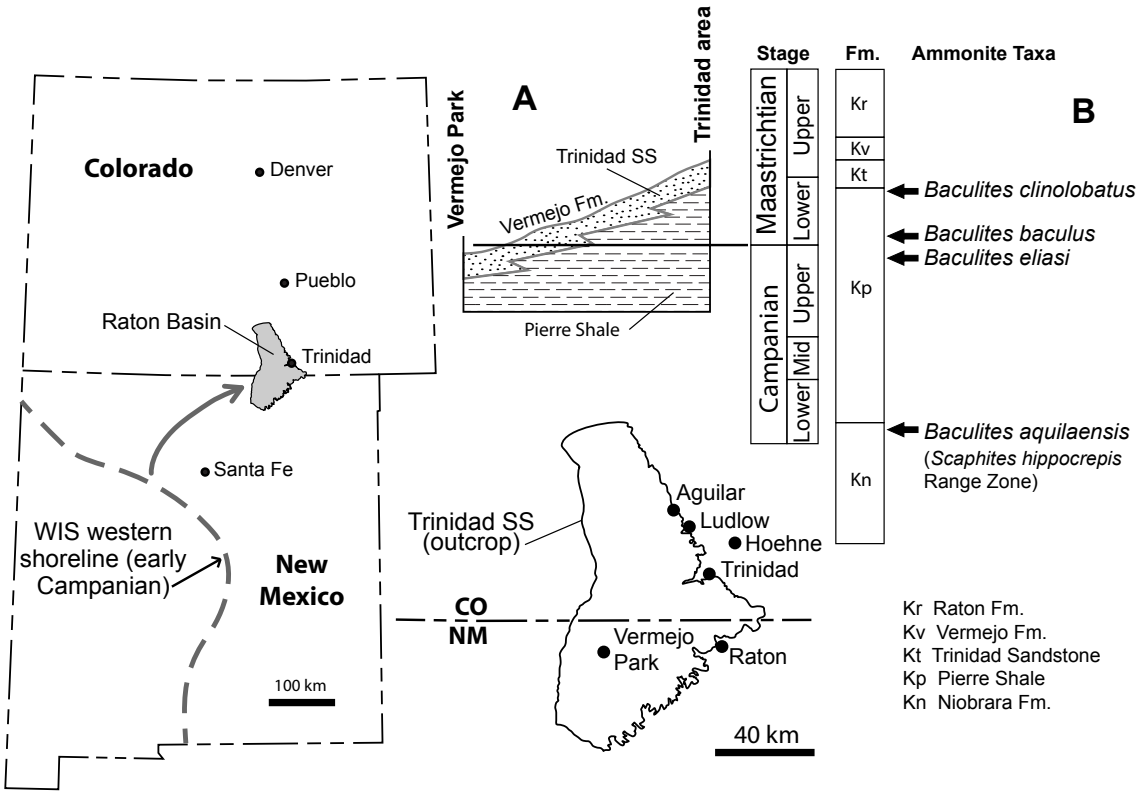

Figure 1. Index map of Raton Basin (left and bottom) showing localities discussed in the text. Approximate outline of the basin is indicated by the Trinidad Sandstone outcrop belt in Colorado and New Mexico. The western shoreline of the Western Interior Seaway (WIS) retreated north and east during Late Campanian-Early Maastrichtian time, as suggested by the arrow on the regional map. Panel A is a sketch depicting the time-transgressive nature of the contact between the Pierre Shale and overlying Trinidad Sandstone, based on biochronologic constraints from the Vermejo Formation near Vermejo Park and from the upper part of the Pierre Shale near Trinidad; the horizontal line represents the Campanian-Maastrichtian stage boundary (ca. 70 Ma). Panel B shows schematically the lithostratigraphic positions of selected species of *Baculites* from the Trinidad area discussed in this paper and in Berry (2016).

Baculites is a genus of straight-shelled ammonites that have been used extensively for biostratigraphic correlation of Upper Cretaceous marine strata (e.g., Klinger and Kennedy, 2001). In previous studies by the author, a sequence of middle Upper Campanian (73.5 Ma) through upper Lower Maastrichtian (69.5 Ma) *Baculites* was reported from the upper part of the Pierre Shale near Ludlow, Colorado (Berry, 2010, 2016; see Fig. 1 for localities mentioned in text). Two species of *Baculites* that provide additional information regarding the age of the Pierre Shale in the vicinity of Trinidad, Colorado are highlighted herein: 1) *B. aquilaensis* from the top of the underlying Niobrara Formation near Hoehne, Colorado; and 2) *B. clinolobatus* from the top of the Pierre Shale at Berwind Canyon near Ludlow, Colorado. The significance of these fossils in the context of the early Laramide history of the region is discussed briefly.

The age of the base of the Pierre Shale

The age of the top of the Niobrara Formation (base of the Pierre Shale) is reasonably well constrained in the southern part of the Raton Basin in northeastern New Mexico, and to the north of the basin near Pueblo, Colorado. Accordingly, the top of the Niobrara Formation in these areas has been placed at or slightly above the top of the Lower Campanian *Scaphites hippocrepis* II Range Zone (Cobban, 1976; Scott, et al., 1986; Merewether et al., 2011), which has an absolute age of about 81.71 ±0.34 Ma (Sageman et al., 2014). However, the age of the contact between the Niobrara Formation and the Pierre Shale is not well constrained in the eastern Raton Basin of south-central Colorado.

The contact between the Pierre Shale and Niobrara Formation is exposed in the vicinity of Hoehne, Colorado (Johnson, 1969). In this general area, the upper beds of the Niobrara Formation (the uppermost, calcareous to sandy shale of the Smoky Hill Member) have been thought to lie within the *Scaphites hippocrepis* faunal zone (Molenaar et al., 2002; Merewether et al., 2011), the base of which is estimated to lie 30 to 35 m below the top of the Niobrara Formation. However, as alluded to above, *Scaphites hippocrepis* may be divided into three morphotypes or subspecies, each representing successive biochrons (from oldest to youngest *S. hippocrepis* I, II, and III; Cobban, 1969); this level of faunal zonation has not been established for the upper part of the Niobrara Formation in the eastern Raton Basin.

Approximately 5 km northeast of Hoehne (sec. 34, T31S, R62W) at New Mexico Museum of Natural History locality 10787 (NMMNH L-10787), the upper 25 to 30 m of the Niobrara Formation (highest, calcareous to sandy shale beds of the Smoky Hill Member) are exposed. Comparison with the Merewether et al. (2011) composite section for the area between Trinidad and Aguilar suggests that these strata probably lie within the Lower Campanian *Scaphites hippocrepis* Zone.

The lowest beds examined at NMMNH L-10787, calcareous shale about 25 m below the top of the Niobrara Formation, contain poorly preserved ammonites of the genus *Haresiceras*. The presence of *Haresiceras* in these beds confirms that these strata lie within the Lower Campanian *Scaphites hippocrepis* Zone (see Cobban, 1964, 1969). Due to their poor state of preservation and fragility, no specimens were collected. Among the poorly preserved *Haresiceras* observed in these beds were fragments that appear to closely resemble *H. placentiforme* Reeside, which has the following diagnostic characteristics (Cobban, 1964): 1) fine, clavate nodes that form a keel; 2) flank ribs that are strongest on the ventrolateral shoulder and that weaken toward the umbilicus; 3) a tightly coiled body chamber with a distinctive, sinuous aperture that takes the shape of the flank ribs; 4) a flattened venter; and (5) subparallel flanks because the phragmocone is narrower than the body chamber. However, some of these characteristics are shared with other species of *Haresiceras* (Cobban, 1964). *H. placentiforme* is characteristic of the *S. hippocrepis* II ammonite biozone (Cobban, 1969; Scott et al., 1986; Sageman et al., 2014), although it does range into the slightly lower *S. hippocrepis* I ammonite biozone (Cobban, 1969). Based on the presence of *H.* cf. *H.*

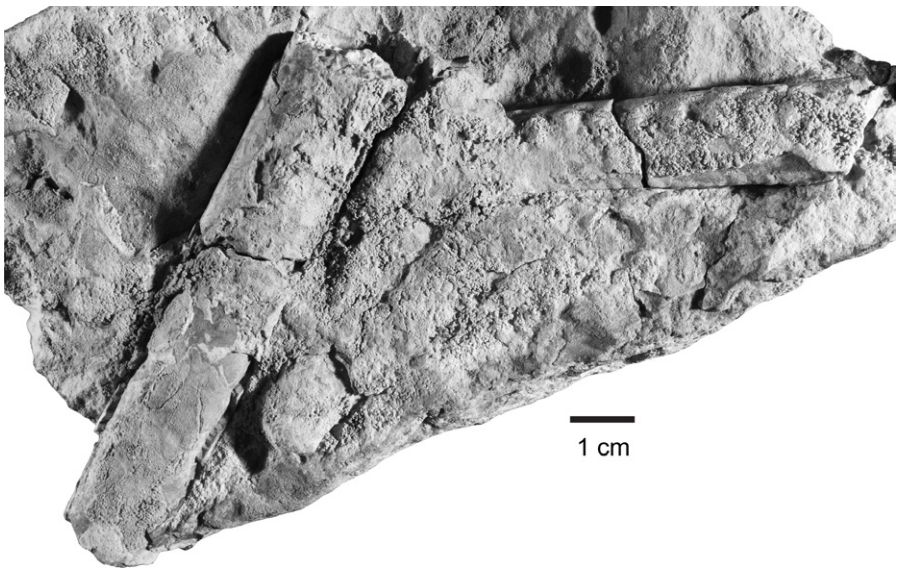

Figure 2. *Baculites aquilaensis* Reeside (NMMNH P-78629) in calcareous, yellow-weathering shale near the top of the Niobrara Formation (NMMNH L-10787). Note the distinctive, arcuate flank ribs on the specimen at the right and the presence of slight ribbing on the venter. *Photograph by P. Sealey.*

placentiforme at NMMNH L-10787, the *S. hippocrepis* II Zone is tentatively thought to lie about 25 m below the top of the Niobrara Formation in this area.

Baculites are locally abundant in strata above the *Haresiceras* beds at NMMNH L-10787, and two specimens were collected from these strata: 1) NMMNH P-78629, which was collected from calcareous shale approximately 15 m below the top of the Niobrara Formation; and 2) NMMNH P-78630, which was collected from sandy shale near the top of the Niobrara Formation. The *Baculites* at NMMNH L-10787 display the following characteristics (Figs. 2, 3): 1) arcuate ribs that take up about half of the flank; 2) an average of about 2.5 to 3 flank ribs per flank diameter; and 3) a slightly ribbed venter. These features are all characteristic of *B. aquilaensis* Reeside (Reeside, 1927; Kennedy, 1993; Klinger and Kennedy, 2001), and the specimens are assigned to that species.

Although *Baculites aquilaensis* is known to range downward into the lowest part of the *Scaphites hippocrepis* Zone (Cobban, 1964), it is more typical of the upper part of the zone (Klinger and Kennedy, 2001). Thus, Kennedy (1993) and Klinger and Kennedy (2001) indicate that *B. aquilaensis* is characteristic of the Lower Campanian *S. hippocrepis* III ammonite biozone, which, according to Harries (2008), ranges from about 81.8–80.5 Ma.

The relative stratigraphic position of the *Haresiceras* beds (about 25 m below the top of the Niobrara Formation) and of the overlying *B. aquilaensis*-bearing beds (about 15–5 m below the top of the Niobrara Formation), suggests that the top of the Niobrara Formation near Hoehne lies slightly above the contact between the *S. hippocrepis* II and *S. hippocrepis* III ammonite range zones.

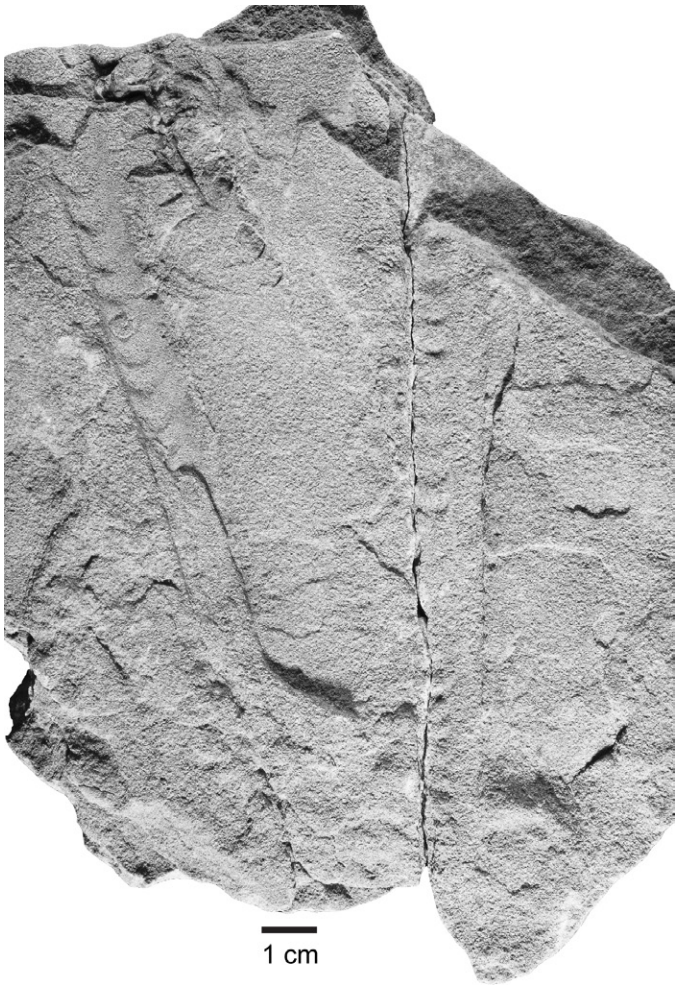

Figure 3. Molds of *Baculites aquilaensis* Reeside (NMMNH P-78630) in sandy shale near the top of the Niobrara Formation (NMMNH L-10787). Note the distinctive, arcuate flank ribs. *Photograph by P. Sealey.*

The age of the top of the Pierre Shale

Previous studies have shown that the top of the Pierre Shale is progressively younger from west to east across the Raton Basin, reflecting the retreat of the Western Interior Seaway from the region during the Late Cretaceous (e.g., Fassett, 1976; Cather, 2004) (Fig. 1). Nearshore-marine deposits of the Trinidad Sandstone were deposited on top of the Pierre Shale in the Raton Basin during the overall regression, followed by terrestrial deposits of the Vermejo and succeeding Raton formations. Palynostratigraphy northwest of Vermejo Park, New Mexico suggests that the Campanian-Maastrichtian stage boundary (70.6 ±0.6 Ma) lies within the Vermejo Formation in that area (Tschudy, 1973), and to the east, near Trinidad, Colorado, the stage boundary lies within the upper part of the Pierre Shale (Merewether et al., 2011; Berry, 2010, 2016) (Fig. 1). Thus, the Raton Basin at approximately 70 Ma was transected by the western shoreline of the Western Interior Seaway (represented by the Trinidad Sandstone), separating it into western terrestrial (Vermejo Formation) and eastern prodeltaic marine (Pierre Shale) depositional environments.

Ammonite biostratigraphy in the vicinity of Trinidad (Merewether et al., 2011; Berry, 2016) indicates that the top of the Pierre Shale in the eastern Raton Basin lies near the Lower-Upper Maastrichtian substage boundary. *Baculites clinolobatus* Elias was reported near the top of the Pierre Shale at Berwind Canyon near Ludlow (Berry, 2016). Prior to that report, the youngest index ammonite reported from the Pierre Shale near Trinidad was *Baculites grandis* Hall and Meek (Merewether et al., 2011). Since the initial report of *B. clinolobatus* from Berwind Canyon (Berry, 2016), an additional collection has been made from the uppermost transitional beds of the Pierre Shale in the same area.

Specimens of *Baculites clinolobatus* (NMMNH P-78603 and P-78625) were collected in Berwind Canyon (NMMNH L-10783; sec. 29, T31S, R64W) from the uppermost transitional unit of the Pierre Shale, which grades into the overlying Trinidad Sandstone. These specimens appear to represent the youngest species of ammonite reported from the Raton Basin thus far, and show that the *B. clinolobatus* zone extends locally into the uppermost, transitional unit of the Pierre Shale. Consequently, the Trinidad Sandstone near its type area in south-central Colorado closely approximates the boundary between the Lower and Upper Maastrichtian, as defined by ammonite zones (Cobban et al., 2006).

Baculites clinolobatus displays several diagnostic features, which are visible on NMMNH P-78603 and P-78625 (Fig. 4): 1) symmetrically bifid lateral lobes (Elias, 1933); 2) an inclined second lateral lobe relative to the long axis of the shell (Elias, 1933; Klinger and Kennedy, 2001); 3) a compressed oval or trigonal cross-section (Elias, 1933); and 4) weak, widely spaced,

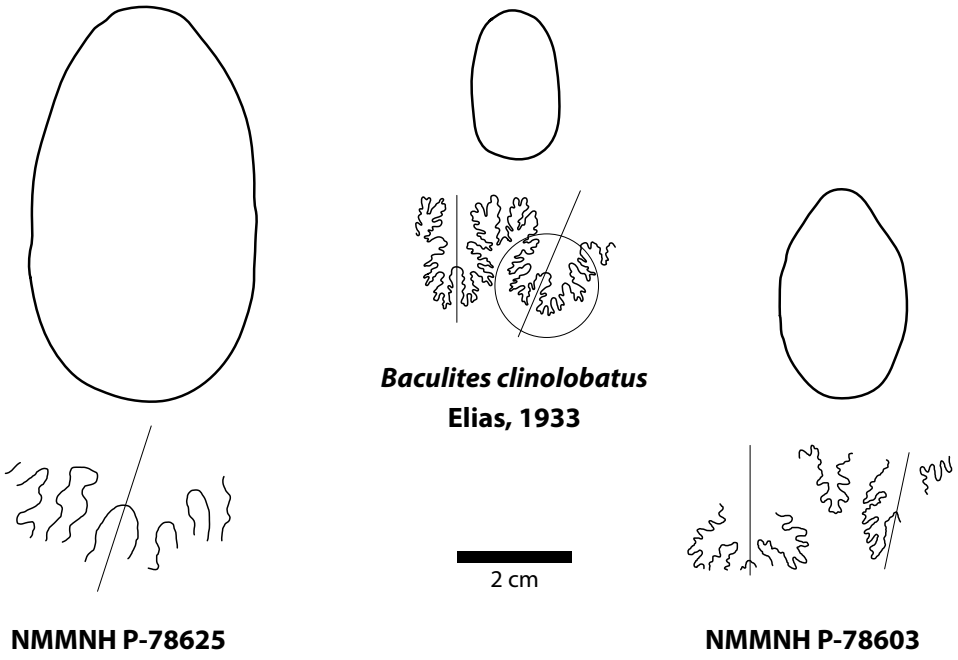

Figure 4. Cross sections and sutures of *Baculites clinolobatus* (NMMNH P-78603, P-78625) collected from the top of the Pierre Shale near Ludlow, Colorado, compared with cotype specimens of *B. clinolobatus* illustrated by Elias (1933, Plate 34, Figs. 1, 2b). Note the diagnostic suture pattern (inclined second lobe is circled) and compressed trigonal cross-section.

low, and broad flank undulations (Gill and Cobban, 1973; not illustrated in Fig. 4). It is distinguished from the closely related forms *B. grandis* Hall and Meek and *B. baculus* Meek and Hayden, which were collected from a stratigraphically lower position in the same area (Berry, 2010, 2016), by its differing cross section, size, and suture pattern (Klinger and Kennedy, 2001).

Discussion and conclusions

The age of the Pierre Shale in the eastern Raton Basin is constrained by the presence of *Baculites aquilaensis* at the top of the Niobrara Formation near Hoehne, Colorado, and by the presence of *B. clinolobatus* at the top of the Pierre Shale near Ludlow. These data indicate that the Pierre Shale ranges from about 80.5–69.5 Ma in the general vicinity of Trinidad, Colorado.

Paleogeographic reconstructions for the Western Interior Basin (e.g., Roberts and Kirschbaum, 1995) show that the western shoreline of the seaway was located south and west of the Raton Basin during Late Santonian to Early Campanian time (Fig. 1). By the mid Late Campanian, the western shoreline had prograded northeastward to the southwestern part of the Raton Basin. The seaway continued its retreat reaching the vicinity of Raton, New Mexico near the end of the Campanian, when it separated the Raton Basin into terrestrial (to the west) and marine (to the east) depositional settings (Fig. 1). By the end of the Maastrichtian, the Western Interior Seaway had completely retreated from the Raton Basin, as recorded by terrestrial deposits of the Vermejo and Raton formations that overlie the Trinidad Sandstone. U-Pb chronology of detrital zircon grains from the Trinidad Sandstone suggests that marine deposition may have extended into the early Paleocene (Bush et al., 2016); however, these data are inconsistent with age constraints derived from index mollusks collected from the Trinidad Sandstone (Berry, 2017) and from the upper part of the underlying Pierre Shale in the eastern part of the Raton Basin (this paper). Although nearby sea-level changes in the Early Paleocene may have influenced the formation of coal in the lower part of the Raton Formation in the eastern Raton Basin (Flores, 1987), no marine fossils of latest Maastrichtian or Paleocene age have been documented from the basin.

The transition from deposition of the Niobrara Formation to deposition of the Pierre Shale probably signaled the beginning of tectonically driven subsidence in the region. If so, apparent similarity in the age of the base of the Pierre Shale north to south across the basin suggests that the onset of subsidence was essentially coincident across this region. Subsequent southwest-to-northeast retreat of the Western Interior Seaway during Late Campanian-Early Maastrichtian time may reflect, at least in part, uplift of the San Luis Highlands just to the west of the Raton Basin (Heller and Liu, 2016). The Trinidad Sandstone and overlying deposits demarcate the transition from a predominantly marine to a predominantly non-marine depositional setting (Flores, 1987; Flores and Pillmore, 1987). The results of the present study indicate that this transition occurred in the eastern Raton Basin near Trinidad during the *B. clinolobatus* biochron at the end of the Early Maastrichtian.

Acknowledgments

The author thanks the following individuals for their contributions to this long-term project: Miranda and Tell Berry, the Tucker-Ball and Berry families, Joshua Slattery, and K.C. McKinney. The assistance of New Mexico Geology editorial staff and constructive reviews by Spencer Lucas and Paul Sealey are acknowledged.

References

Baltz, E.H., 1965, Stratigraphy and history of Raton basin and notes on San Luis basin, Colorado-New Mexico: Bulletin of the American Association of Petroleum Geologists, v. 49, p. 2041–2075.

Berry, K., 2010, Contributions to the marine stratigraphy of Berwind Canyon, southeastern Colorado: The Mountain Geologist, v. 47, p. 59–69.

Berry, K., 2016, Biostratigraphy of the Campanian-Maastrichtian, mid-Maastrichtian, and Cretaceous-Tertiary boundaries in the Raton Basin: implications for models of early Laramide tectonism and for the origin of the enigmatic Disturbed Zone: The Mountain Geologist, v. 53, p. 75–91.

Berry, K., 2017, New paleontological constraints on the paleogeography of the Western Interior Seaway near the end of the Cretaceous (late Campanian–Maastrichtian) with a special emphasis on the paleogeography of southern Colorado, U.S.A.: Rocky Mountain Geology, v. 52, p. 1–16.

Bush, M.A., Horton, B.K., Murphy, M.A., and Stockli, D.F., 2016, Detrital record of initial basement exhumation along the Laramide deformation front, southern Rocky Mountains: Tectonics, v. 35, p. 2117–2130.

Cather, S.M., 2004, Laramide orogeny in central and northern New Mexico and southern Colorado: New Mexico Geological Society, Special Publication 11, p. 203–248.

Cobban, W.A., 1964, The Late Cretaceous cephalopod *Haresiceras* Reeside and its possible origin: United States Geological Survey, Professional Paper 454-I, 16 p.

Cobban, W.A., 1969, The Late Cretaceous *ammonites Scaphites leei* (Reeside) and *Scaphites hippocrepis* (DeKay) in the Western Interior of the United States: United States Geological Survey, Professional Paper 619, 23 p.

Cobban, W.A., 1976, Ammonite record from the Pierre Shale of northeastern New Mexico: New Mexico Geological Society, Guidebook 27, p. 165–169.

Cobban, W.A., Walaszczyk, I., Obradovich, J.D., and McKinney, K.C., 2006, A USGS zonal table for the Upper Cretaceous Middle Cenomanian-Maastrichtian of the Western Interior of the United States based on ammonites, inoceramids, and radiometric ages: United States Geological Survey, Open-File Report 2006-1250, 46 p.

Elias, M.K., 1933, Cephalopods of the Pierre Formation of Wallace County, Kansas, and adjacent areas: University of Kansas Science Bulletin, v. 21, p. 289–363.

Fassett, J.E., 1976, What happened during Late Cretaceous time in the Raton and San Juan basins—with some thoughts about the area in between: New Mexico Geological Society, Guidebook 27, p. 185–190.

Flores, R.M., 1987, Sedimentology of Upper Cretaceous and Tertiary siliciclastics and coals in the Raton Basin, New Mexico and Colorado: New Mexico Geological Society, Guidebook 38, p. 255–264.

Flores, R.M., and Pillmore, C.L., 1987, Tectonic control on paleoarchitecture of the Cretaceous and Tertiary Raton Basin, Colorado and New Mexico, *in* Ethridge, F.G., Flores, R.M., and Harvey, M.D. eds., Recent Developments in Fluvial Sedimentology: Society of Economic Paleontologists and Mineralogists, Special Publication 39, p. 311–321.

Gill, J.R. and Cobban, W.A., 1973, Stratigraphy and geologic history of the Montana Group and equivalent rocks, Montana, Wyoming, and North and South Dakota: United States Geological Survey, Professional Paper 776, 37 p.

Harries, P.J., 2008, A reappraisal of the relationship between sea level and species richness, *in* Harries, P.J., ed., High-resolution Approaches in Stratigraphic Paleontology: New York, Springer Science, p. 227–263.

Heller, P.L. and Liu, L., 2016, Dynamic topography and vertical motion of the U.S. Rocky Mountain region prior to and during the Laramide orogeny: Geological Society of America Bulletin, v. 128, p. 973–988.

Johnson, R.B., 1969, Geologic map of the Trinidad Quadrangle: USGS Miscellaneous Investigations Map I-558, scale 1:250,000.

Kennedy, W.J., 1993, Campanian and Maastrichtian ammonites from the Mons Basin and adjacent areas (Belgium): Sciences de la Terre, v. 63, p. 99–131.

Klinger, H.C., and Kennedy, W.J., 2001, Stratigraphic and geographic distribution, phylogenetic trends and general comments on the ammonite family Baculitidae Gill, 1871 (with an annotated list of species referred to the family): Annals of the South African Museum, v. 107, 290 p.

Lee, W.T., 1917, Geology of the Raton Mesa and other regions in Colorado and New Mexico, *in* Lee, W.T., and Knowlton, F.H., eds., Geology and Paleontology of the Raton Mesa and Other Regions, Colorado and New Mexico: United States Geological Survey, Professional Paper 101, p. 9–223.

Merewether, E.A., Cobban, W.A., and Obradovich, J.D., 2011, Biostratigraphic data from Upper Cretaceous formations—Eastern Wyoming, Central Colorado, and Northeastern New Mexico: United States Geological Survey, Scientific Investigations Map 3175, 10 p., 2 sheets.

Molenaar, C.M., Cobban, W.A., Merewether, E.A., Pillmore, C.L., Wolfe, D.G., and Holbrook, J.M., 2002, Regional stratigraphic cross sections of east-central Arizona to the Oklahoma Panhandle: United States Geological Survey, Miscellaneous Field Studies Map MF-2382.

Reeside, J.B., 1927, The cephalopods of the Eagle Sandstone and related formations in the Western Interior of the United States: United States Geological Survey, Professional Paper 151, 87 p.

Roberts, L.N.R., and Kirschbaum, M.A., 1995, Paleogeography of the Late Cretaceous of the Western Interior of middle North America coal distribution and sediment accumulation: United States Geological Survey, Professional Paper 1561, 115 p.

Sageman, B.B., Singer, B.S., Meyers, S.R., Siewart, S.E., Walaszczyk, I., Condon, D.J., Jicha, B.R., Obradovich, J.D., and Sawyer, D.A., 2014, Integrating $^{40}Ar/^{39}Ar$, U-Pb, and astronomical clocks in the Cretaceous Niobrara Formation, Western Interior Basin, USA: Geological Society of America Bulletin, v. 126, p. 956–973.

Scott, G.R., Cobban, W.A., and Merewether, F.A., 1986, Stratigraphy of the Upper Cretaceous Niobrara Formation in the Raton Basin, New Mexico: New Mexico Bureau of Mines and Mineral Resources, Bulletin 115, 34 p.

Slattery, J.S., Cobban, W.A., McKinney, K.C., Harries, P.J., and Sandness, A.L., 2015, Early Cretaceous to Paleogene paleogeography of the Western Interior Seaway: The interactions of eustasy and tectonism, *in* Bingle-Davis, M., ed., Wyoming Geological Association 68th Annual Field Conference Guidebook, Casper, WY, p. 22–60.

Tschudy, R.H., 1973, The Gasbuggy core: A palynological appraisal, *in* Fassett, J.E., ed., Cretaceous and Tertiary rocks of the Southern Colorado Plateau: Durango, CO, Four Corners Geological Society, p. 131–143.

Revised basin geometry for the Bursum Formation (upper Virgilian-lower Wolfcampian), central New Mexico

Steven M. Cather
New Mexico Bureau of Geology and Mineral Resources
New Mexico Institute of Mining and Technology, Socorro, NM 87801

Abstract

The Bursum Formation of latest Pennsylvanian age was deposited during the final episode of the Ancestral Rocky Mountains deformation in central New Mexico. Over 600 paleocurrent measurements were collected from fluvial strata of the Bursum Formation in the Quebradas region east of Socorro. These measurements, in concert with data from the Bursum Formation for thickness (from outcrops and wells), lithofacies distribution, and maximum clast size provide new constraints on the paleotectonic framework during the Late Pennsylvanian. The long-known Joyita Uplift supplied detritus, mostly recycled from older Pennsylvanian strata, to the northern part of the study area. A major source region exposing dominantly Proterozoic rocks, herein termed the San Antonio Uplift, existed in what is now the southern part of the Socorro Basin of the Rio Grande rift. The San Antonio Uplift contributed arkosic detritus to the central and southern parts of the study area. These two uplifts dominated sediment supply to the western part of a broad region in which the Bursum Formation gradually thickens to the southeast, toward the Pedernal Uplift near Carrizozo. This region formed a weakly subsided saddle-shaped platform between the deep Estancia and Pedernal basins to the north and south. It was not a narrow, symmetrical basin as depicted in previous studies.

Introduction

The Bursum Formation is an interval of continental and marine beds transitional between the underlying Pennsylvanian marine strata of the Atrasado Formation (upper Madera Group) and the overlying continental red beds of the Permian Abo Formation in central New Mexico. The Bursum Formation was first proposed by Wilpolt et al. (1946), who designated the type section in the Hansonburg Hills (SE 1/4 sec. 1, T6S, R4E), about 45 km southeast of Socorro, New Mexico. The present study area involves Bursum Formation exposures on six quadrangles in the Quebradas region east of Socorro (Fig. 1). These quadrangles are the Bustos Well (Cather et al., 2014), Cañon Agua Buena (Cather et al., 2007), Loma de las Cañas (Cather and Colpitts, 2005), Mesa del Yeso (Cather et al., 2004), San Antonio (Cather, 2002), and the Sierra de la Cruz (Cather et al., 2012). I also compiled Bursum thickness data from the analysis of cuttings and geophysical logs from petroleum exploration wells by Broadhead (1997) and Broadhead and Jones (2004), and I conducted additional field studies in the Joyita Hills, near Abo Pass, and south of Little San Pascual Mountain.

The Bursum Formation consists of variegated greenish-gray and purplish-red beds of mudstone, marine limestone, sandstone, conglomerate, and calcic pedogenic horizons (Fig. 2). The Bursum commonly exhibits cyclic alternation of continental and marine beds. These beds define regressive-transgressive sequences ~10–50 m thick and reflect both eustatic and tectonic processes (Krainer and Lucas, 2009). Bedding in the Bursum Formation is typically laterally discontinuous. The basal parts of aggradational sequences are commonly confined within shallow paleovalleys or inset paleochannels 0.1–1.5 km wide (Fig. 3). Beds in the Bursum are generally not traceable for more than a kilometer or two, making correlation among discontinuous exposures difficult.

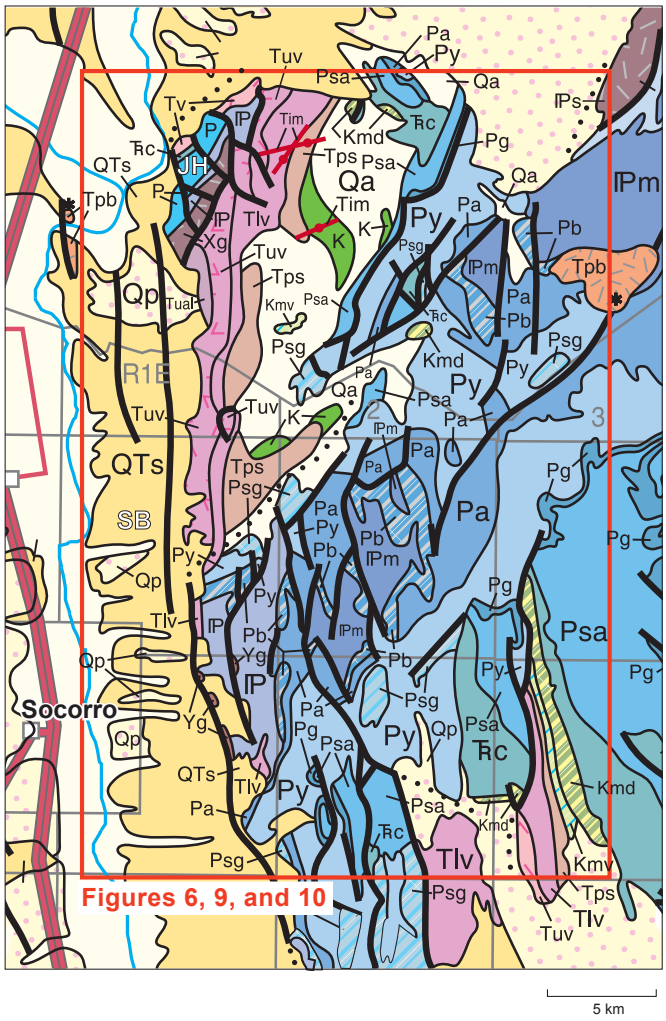

Figure 1. Simplified geologic map of the east flank of the Socorro Basin (SB) of the Rio Grande rift, showing the area of Figures 6, 9, and 10 (rectangle). The Joyita Hills (JH) are a remnant of the Pennsylvanian Joyita Uplift. Base map is from New Mexico Bureau of Geology and Mineral Resources (2003) Geologic Map of New Mexico. Bursum Formation exposures are labeled Pb, except in northwestern part of the map where they are included in the upper part of unit IP. See New Mexico Bureau of Geology and Mineral Resources, 2003, Geologic Map of New Mexico, scale 1:500,000, two sheets for symbols and other unit labels.

Figure 2. Interbedded fluvial sandstone and marine limestone in the lower part of the Bursum Formation. Hammer rests on arkosic pebbly fluvial sandstone, which is overlain by a transgressive succession of ~1.5 m of gray marine? siltstone and ~0.3 m of gray marine limestone (upper ledge). View is toward the east from 13S 0336949E, 3760462N, ~1.3 km north of the Cerro del Viboro measured section of Krainer and Lucas (2009), San Antonio quadrangle. All UTM data are NAD 1927.

Figure 3. Shallow paleovalley or paleochannel fills containing arkosic, pebbly sandstone in lower part of Bursum Formation. The channel deposit in the foreground (with hammer for scale) is about 0.5 m thick and 2 m wide. Larger valley-fill above and to the right (above gray bushes) is about 1.5 m thick and 10 m wide. Generally, paleovalley fills in the Bursum are thicker and wider than these, but are more difficult to photograph. View is toward the east (subparallel to the paleoflow direction) from near 13S 0337000E, 3760410N, ~1.3 km north of the Cerro del Viboro measured section of Krainer and Lucas (2009), San Antonio quadrangle.

Lucas and Krainer (2004) and Krainer and Lucas (2009, 2013) subdivided the Bursum laterally into four members (Oso Ridge, Bruton, Red Tanks and Laborcita members; note that the last three have at times been considered formation-rank terms). Not strictly lithostratigraphic in nature, these members are based on the ratio of marine to continental beds, overall thickness, and grain size. The range of lithologic characteristics for individual members has not been defined quantitatively, and member names have not been applied in a systematic fashion. For example, the Bursum strata of the Tinajas Arroyo measured section of Krainer and Lucas (2009) were classified as the Bruton Member (i.e., containing >50% marine strata; Lucas and Krainer, 2004, p. 44), despite only containing ~38% marine beds by their own estimation. The Bursum Formation is not subdivided in the present study.

The age of the Bursum Formation in central New Mexico, determined mostly from fossils within marine limestones, ranges from late Virgilian to early Wolfcampian (Krainer and Lucas, 2013). The Bursum Formation is regionally somewhat time-transgressive (Lucas and Krainer, 2004; Krainer and Lucas, 2009, 2013), and the contact between the Bursum and the overlying Abo Formation approximates the Pennsylvanian–Permian boundary as construed by Davydov et al. (1998; see summary in Lucas et al., 2016). Within the study area, age constraints are sparse. In the northern part of the study area near Cibola Spring, Allen et al. (2013) reported late Virgilian? fusulinids (*Triticites*) in the lower part of the Bursum and early Wolfcampian fusulinids (*Schwagerina* and *Triticites*) in its middle part. Also from the lower and middle Bursum near Cibola Spring, Kottlowski and Stewart (1970; their Palo Duro Canyon section in sec. 13, T1S, R2E, projected) reported *Swagerina emaciata, S. jewetti, S. grandensis, S.* cf. *pinosensis, Stewartina* spp., *Triticites hugensis, T. ventricosus, T.* n. sp., and *Oketaella?*. The Wolfcampian fusulinid *Triticites creekensis* was collected by Maulsby (1981) in the central part of the study area. In a study spanning Bursum outcrops throughout the Quebradas area, Altares (1990) reported the Wolfcampian fusulinids *Schwagerina pinosensis, Triticites* aff. *T. creekensis, T.* cf. *Triticites directus,* and *Leptotriticites sp.* Except for *S. pinosensis,* all were collected within 10 m of the base of the Bursum Formation.

The Bursum Formation unconformably overlies the Virgilian Moya Member of the Atrasado Formation throughout most the study area (Krainer and Lucas, 2009). The associated lacuna appears to encompass part or all of late Virgilian time, representing perhaps a few million years or less. The late Virgilian was a time of eustatic sea-level fall (e.g., Montañez and Poulsen, 2013, their fig. 2g), which may partly account for the sub-Bursum unconformity. Eustatic effects, however, are difficult to prove, particularly given the clear evidence in New Mexico for tectonism at this time. For example, north of the study area along the western flank of Pennsylvanian Joyita Uplift, the Bursum laps across tilted and beveled rocks of Missourian, Desmoinesian, Atokan, and Proterozoic age (Kottlowski and Stewart, 1970). This angular unconformity must be, at least in part, tectonic in origin. To the south, the Bursum Formation in the study area is defined by the first occurrence of reddish continental deposits above the marine Moya Member of the Atrasado Formation. This contact is typically sharp and unconformable. The unconformity at the base of the Bursum Formation represents perhaps the only substantial regional lacuna during Pennsylvanian–Permian sedimentation in the study area.

The nature of the upper contact of the Bursum Formation in the Quebradas region varies locally. I have seen evidence for both disconformable and conformable contacts with the overlying Abo Formation, as did Colpitts (1986) and Altares (1990). Other workers have interpreted the upper contact with the Abo to be gradational (Rejas, 1965; Kottlowski and Stewart, 1970; Arendt, 1971; Maulsby, 1981). In particular, there is no evidence within the six-quadrangle map area for significant soil development or deep ravinement beneath the Abo Formation, which suggests the Bursum–Abo contact represents at most a short lacuna.

In contrast, Krainer and Lucas (2009) interpreted the Bursum–Abo contact to be everywhere unconformable in the Quebradas region. This interpretation is based on their anomalously thick measured section at Gallina Well, which contains six unconformity-bounded depositional sequences. To explain the fewer sequences (three or less) present in their other, thinner measured sections, Krainer and Lucas (2009) invoked the effects of deep pre-Abo erosion. The Gallina Well section, however, may be fault-repeated (see below). Even if it is not, the increased number of depositional cycles in the Gallina Well section may simply reflect increased syndepositional subsidence relative to adjacent areas, rather than pre-Abo erosion. During my mapping of this region, I saw no evidence for more than a few meters of stratigraphic relief on the Bursum–Abo contact.

Ideally, the upper contact of the Bursum Formation is placed at the top of the stratigraphically highest marine limestone or mudstone beneath the Abo. In practice, however, the top of the Bursum is commonly placed within non-marine sandstones and mudstones, at a color change from greenish-gray and grayish- or purplish-red in the Bursum Formation to red and reddish-brown in the Abo. For example, in the Loma de las Cañas and Mesa del Yeso measured sections of Krainer and Lucas (2009), the top of the Bursum consists of non-marine beds, and their Joyita Hills B section is entirely non-marine. The uppermost parts of most Bursum Formation sections measured by Kottlowski and Stewart (1970) also consist of non-marine strata.

Paleocurrent analysis

Unlike the most of the underlying Pennsylvanian succession, the Bursum Formation is widely exposed in the study area and contains coarse clastic deposits that are amenable to paleocurrent analysis. A paleocurrent study was therefore undertaken to provide insight into the latest Carboniferous paleogeography and sediment dispersal systems. Most measurements are from bedload-dominated, probably braided, stream deposits. About 650 paleocurrent measurements from 12 localities were made in Bursum fluvial sandstones within and near the study area (Fig. 4). Nearly all were derived from the structurally restored (i.e., untilted) foreset dip-directions of tabular cross-bedding in sandstones (Fig. 5; this cross-bedding mostly reflects the downstream migration of subaqueous dunes within fluvial channels). The remainder (~7 %) is from trough cross-bedding and pebble imbrication.

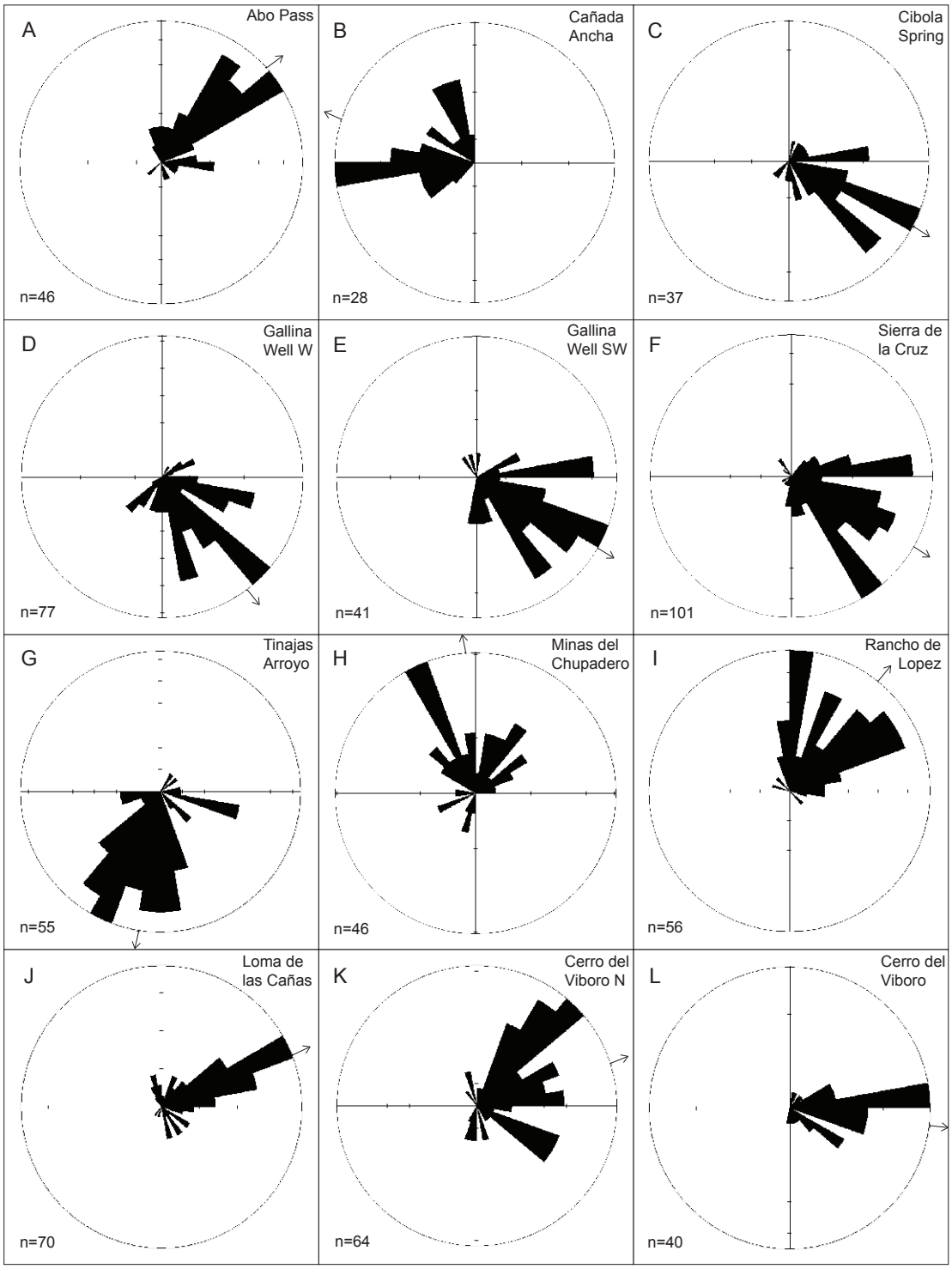

Figure 4. Paleocurrent data (north at top) and mean paleocurrent directions (arrows) for the Bursum Formation exposures in the study area and in surrounding areas. **A**—middle part of Bursum Formation near Abo Pass in roadcuts along US-60, measurements from 13S 0361994E, 3807769N and westward for ~300 m; **B**—upper part of Bursum Formation in the Los Cañoncitos area south of Cañada Ancha, near 13S 0333137E, 3796382N; **C**—lower and middle parts of Bursum Formation ~1 km southwest of Cibola Spring, measurements from 13S 0345147E, 3788062N and westward for ~1 km; **D**—lower part of Bursum Formation ~1.5 km west of Gallina Well, measurements from 13S 0341017E, 3779585 and north-northwestward for ~400 m; **E**—lower part of Bursum Formation ~2 km southwest of Gallina Well, measurements from 13S 0340740E, 3778278N and southward for ~400 m; **F**—middle and upper parts of Bursum Formation ~3.2 km south of Sierra de la Cruz, measurements from 13S 0343734E, 3780095N and southeastward for ~500 m; **G**—lower and middle parts of Bursum Formation near Tinajas Arroyo section of Krainer and Lucas (2009), measurements from 13S 0340764E, 3775876N and southwestward for ~400 m; **H**—lower and middle parts of Bursum Formation near Minas del Chupadero, measurements from 13S 0332266E, 3775595N and eastward for ~300 m; **I**—lower, middle, and upper parts of Bursum Formation ~2.3 km south of Rancho de Lopez, measurements from 13S 0335787E, 3772676N and southward for ~1.7 km; **J**—lower and middle parts of Bursum Formation near the Loma de las Cañas section of Krainer and Lucas (2009), measurements from 13S 0338387E, 3771413N and north-northeastward for ~300 m; **K**—lower and middle parts of Bursum Formation ~1.3 km north of Cerro del Viboro section of Krainer and Lucas (2009), measurements from 13S 0337119E, 3760568N and southward for ~300 m; **L**—lower and middle parts of Bursum Formation near the Cerro del Viboro section of Krainer and Lucas (2009), measurements from the area around 13S 03337293E, 37592251N.

Figure 5. Crossbedding in the middle part of the Bursum Formation along Cañoncito de la Uva, near the Sierra de la Cruz measured section of Krainer and Lucas (2009). View to southwest from 13S 0343736E, 3780090N, Sierra de la Cruz quadrangle.

Not incorporated into the present study are paleocurrent measurements by Altares (1990), who collected relatively few measurements, some of which are based on features of dubious utility such as ripple cross laminations and the orientation of plant fragments.

In the present study, paleocurrents for individual localities typically display unimodal or closely-grouped polymodal distributions. The lack of polar bimodality suggests little or no tidal or estuarine influence during deposition of Bursum fluvial sandstones.

Two broad, semi-radial arrays of fluvial paleocurrent directions are present in the Bursum Formation within, and north of, the study area (Fig. 6). The southern array corresponds to notably arkosic Bursum exposures in the southern part of the study area in which pebbles consist mostly of Proterozoic lithologies (granite, gneissic granite, and vein quartz, with minor schist and greenstone; Fig. 7) with subsidiary, mostly intraformational carbonate clasts. The semi-radial easterly to northerly paleocurrents within this basement-derived petrofacies suggest Proterozoic exposures existed in what is now the southern part of the Socorro Basin of the Rio Grande rift. Herein, this source terrane is termed the San Antonio Uplift.

The northern semi-radial array of southeasterly to southerly paleocurrents corresponds to dominantly subarkosic to calcarenitic fluvial sandstones (e.g., point-count data in Colpitts, 1986) in which pebbles are mostly limestone and siltstone (Fig. 8); basement-derived pebbles are a minor constituent. Deposits of the northern semi-radial array are interpreted to represent a distributive fluvial system (e.g., Weissmann et al., 2010) in which sand and gravel were derived primarily from recycling of Pennsylvanian deposits, particularly the upper Madera Group. Reworking of upper Madera deposits may explain the differing composition of Bursum conglomerates and sandstones in the northern part of the study area—pebbles were derived mostly from indurated Madera limestones, but most sand was recycled from weakly indurated Madera subarkosic sandstones. The northern

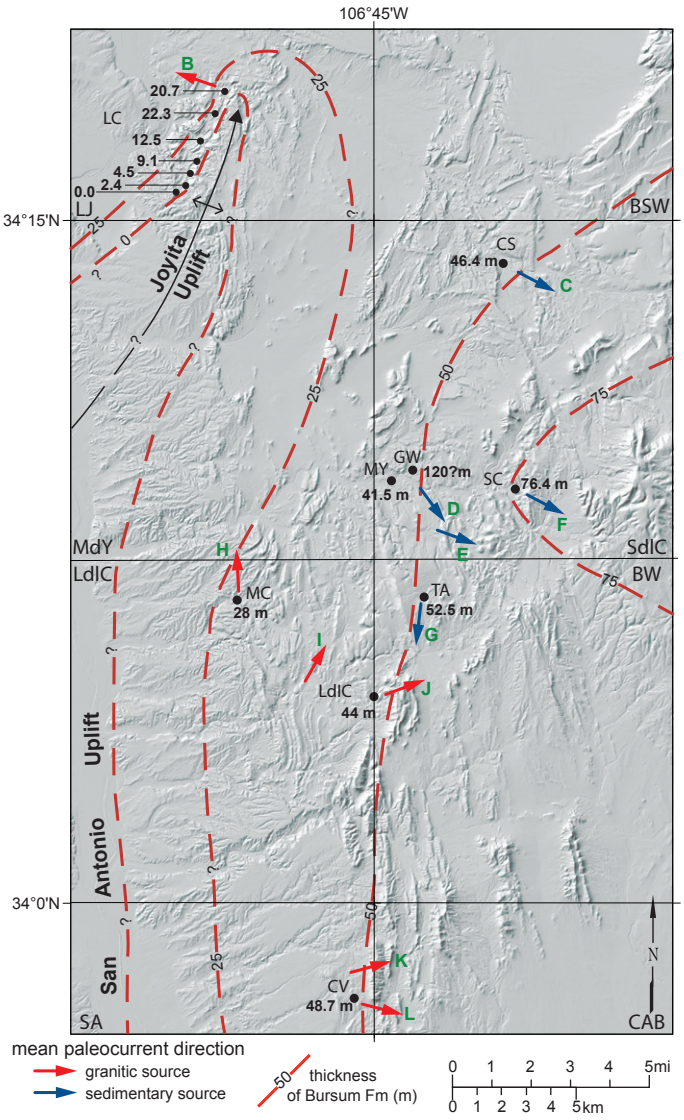

Figure 6. Digital elevation map showing modern topography and average paleocurrent directions (green letters are keyed to Fig. 4) and thickness for the Bursum Formation. Names of measured sections are modified from Krainer and Lucas (2009; note that several of their sections were incorrectly located on their maps and have been replotted here and on subsequent figures). LC—Los Cañoncitos; CS—Cibola Spring; MY—Mesa del Yeso; GW—Gallina Well; SC—Sierra de la Cruz; MC—Minas del Chupadero; TA—Tinajas Arroyo; LdlC—Loma de las Cañas; CV—Cerro del Viboro. Thicknesses are averaged for localities in which more than one section has been measured. These localities include Cibola Spring (average of 52.7 m measured by Altares, 1990, and 40 m by Allen et al., 2013), Mesa del Yeso (average of 57.9 m maximum thickness measured by Kottlowski and Stewart, 1970, and 25 m by Krainer and Lucas, 2009, their fig. 3), Sierra de la Cruz (average of 88.1 m measured by Altares, 1990, 78 m by Krainer and Lucas, 2009, and 63.2 m by Colpitts, 1986), Tinajas Arroyo (average of 51.9 m measured by Altares, 1990, and 53 m by Krainer and Lucas, 2009), Loma de las Cañas (average of 41.3 m measured by Altares, 1990, 54 m by Krainer and Lucas, 2009, and 36.7 m by Maulsby, 1981), and Cerro del Viboro (average of 41 m measured by Altares, 1990, 46 m by Krainer and Lucas, 2009, and 59 m by Fagrelius, 1982). Thicknesses at Los Cañoncitos are from Kottlowski and Stewart (1970) and those near Minas del Chupadero and Gallina Well are from Krainer and Lucas (2009, their fig. 5). The anomalous 120 m thickness near Gallina Well was not contoured (see text). Quadrangle abbreviations are Becker SW (BSW), Bustos Well (BW), Cañon Agua Buena (CAB), La Joya (LJ), Loma de las Cañas (LdlC), Mesa del Yeso (MdY), San Antonio (SA), and Sierra de la Cruz (SdlC).

Figure 7. Basement-derived clasts typical of pebble suites in Bursum outcrops in the southern part of the study area, consisting mostly of gneissic granite and quartzite. Note schist clast near pen tip. The angularity of the fragile schist clast suggests a proximal source. Outcrop photo from near the Cerro del Viboro section of Krainer and Lucas (2009), San Antonio quadrangle.

Figure 8. Typical fluvial pebble suite from the Bursum Formation in the northern part of the study area. Note dominance of clasts of Pennsylvanian limestone (gray) and siltstone (yellow-orange). The sandstone in the upper part of the photo is calcarenitic. Outcrop is in the lower part of the Bursum Formation near Cibola Spring (13S 0344943E, 3788457N), Sierra de la Cruz quadrangle.

array appears to have emanated from the Joyita Uplift. Northeast of the study area near Abo Pass, paleocurrent indicators in Bursum exposures along US-60 show paleoflow was toward the northeast (Fig. 4A), similar to results of Krainer et al. (2009). The Abo Pass deposits also appear to have been derived from the Joyita Uplift, based on their sediment dispersal pattern.

In the Los Cañoncitos area on the western flank of the Joyita Uplift, Bursum fluvial deposits consist mostly of arkosic sandstone and conglomerate which contain Proterozoic clasts and, less commonly, Pennsylvanian limestone pebbles (Kottlowski and Stewart, 1970). Limited paleocurrent data from the upper part of the Bursum near section JH1 of Kottlowski and Stewart (1970) suggest paleoflow was toward the west-northwest (Fig. 4B).

Isopach trends

The thickness of the Bursum Formation, based on 15 measured sections by previous workers in the study area, ranges from about 25 to possibly 120 m. Figure 6 shows the contoured distribution of the averaged measured thicknesses of the Bursum Formation from previous studies. Because thicknesses measured within individual exposures vary among workers, the average measured thickness for each locality is presented in Figure 6. The reasons for the differences between measured thicknesses are unclear. Possibilities include actual thickness differences, differing placement of contacts, and a varying appreciation of structural complications between workers.

North of the study area, on the west flank of the Joyita Uplift, the Bursum ranges from 0 to 22 m thick in seven measured sections, thickening rapidly away from the uplift (Kottlowski and Stewart, 1970). Southeast of the uplift, the Bursum Formation thickens gradually and monotonically eastward. An exception is the anomalously thick (120 m) section measured by Krainer and Lucas (2009) near Gallina Well. In my opinion, this section likely represents a fault-repeated section (see citation of R. Colpitts, 2009, written communication, in Krainer and Lucas, 2009, p.168, for a similar opinion). The anomalous thickness of the Gallina Well section is illustrated by nearby, thinner measured sections in the Bursum Formation.

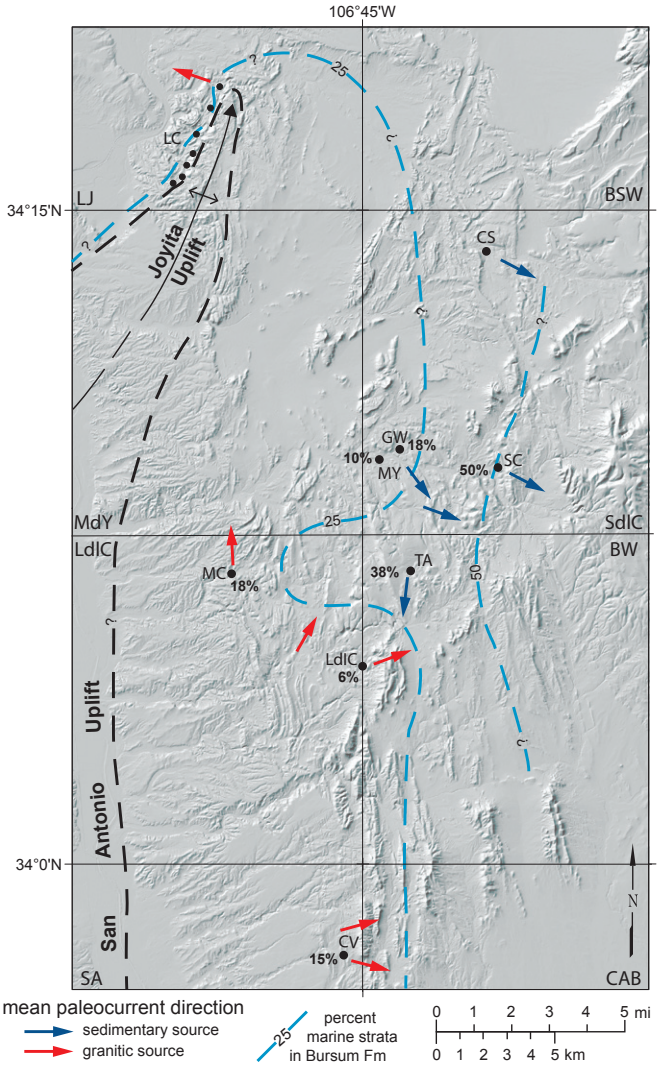

Figure 9. Digital elevation map showing average paleocurrent directions (from Fig. 4) and percentage of marine strata in Bursum Formation, compiled from the interpretations of Krainer and Lucas (2009, 2013). Percentage of marine strata in the Los Cañoncitos area west of Joyita Uplift is estimated from the lithologic descriptions of Kottlowski and Stewart (1970). Abbreviations are defined in Figure 6.

About 1.1 km west of the Gallina Well section, Krainer and Lucas (2009, their fig. 3) measured only 25 m of Bursum in their Mesa del Yeso section (note that the Gallina Well and Mesa del Yeso measured section locations are transposed on their fig. 1). Kottlowski and Stewart (1970, p. 23) measured no more than 57.9 m nearby to the west. Not contoured in Figure 6, the 120 m thickness of the Gallina Well section, if correct, would require a local, deeply subsided sub-basin within the study area.

Proportion of marine strata

Figure 9 shows the percentage of marine strata within ten measured sections of the Bursum Formation, based on the paleoenvironmental interpretations of Krainer and Lucas (2009). East of the Joyita and San Antonio uplifts, the abundance of marine rocks in the Bursum increases rather systematically eastward, as noted by Krainer and Lucas (2009). A westward embayment in the 25% marine contour approximately coincides with the area between the two semi-radial distributive fluvial systems defined above.

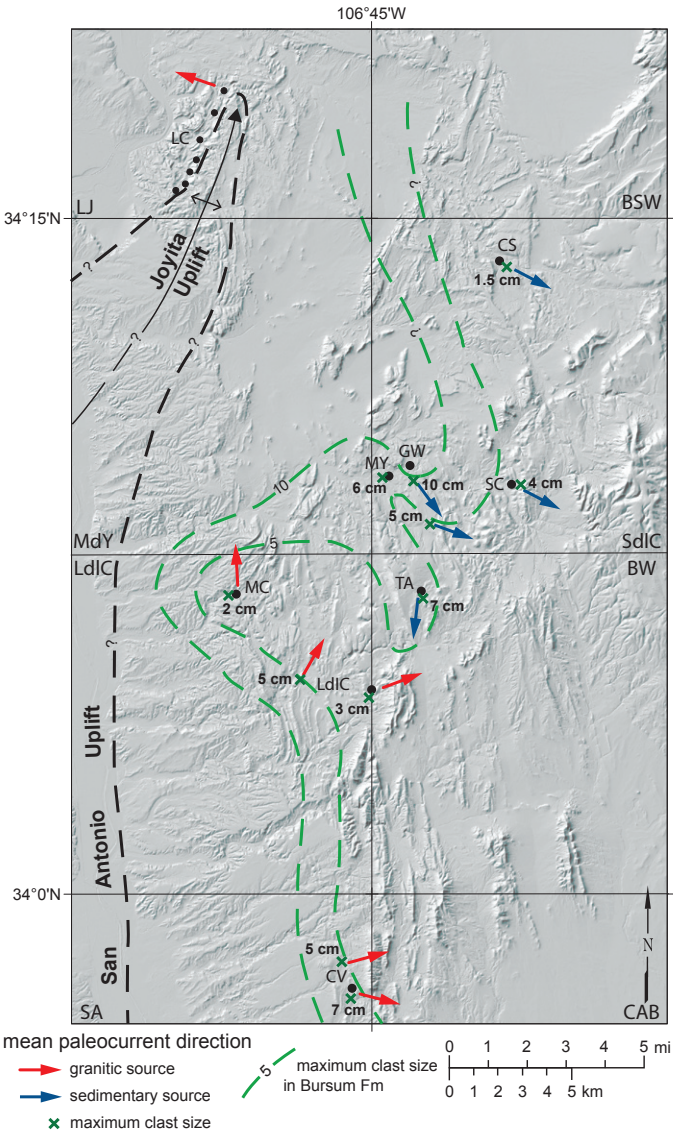

Figure 10. Digital elevation map of modern topography showing average paleocurrent directions (from Fig. 4) and maximum clast-size distribution for Bursum outcrops in the study area. Abbreviations are defined in Figure 6.

The increased percentage of marine strata in this area probably reflects a paleotopographic low area between two constructional lobes in which marine flooding was more frequent or persistent.

Maximum clast-size distribution

Maximum clast-size data, based on the average of the ten largest clasts observed at each locality, were collected from fluvial beds within the study area (Fig. 10). The measured clasts were mostly vein quartz in the south, and limestone in the north. These data define a fine-grained area between the two distributive fluvial systems, and suggest lower fluvial paleogradients existed in the intervening embayment. No systematic study of maximum clast size was attempted in the Los Cañoncitos area west of the Joyita Uplift. Kottlowski and Stewart (1970) reported clasts as large as cobbles in that area. No pebbles other than intraformational rip-up clasts were observed in the Abo Pass or Little San Pascual Mountain outcrops.

Regional structure and paleogeography

Paleocurrent data and the dominance of north-south contours of thickness, percent marine strata, and maximum clast size in the Bursum Formation (Figs. 6, 9, and 10) in the study area are not compatible with derivation solely from the Joyita Uplift, but instead suggest a Late Paleozoic uplift (the San Antonio Uplift) occupied much of the southern Socorro Basin. Although shown as being contiguous with the Joyita Uplift, available data also allow that the San Antonio Uplift was separated from the Joyita Uplift by a topographically low area north of the town of Socorro.

The Joyita Uplift has been depicted by most workers as a small positive feature with a paleogeographic extent similar to that of the present outcrops of Proterozoic rocks in the Joyita Hills, but its original Pennsylvanian geometry is partly obscured by subsequent Laramide and rift tectonism. The western flank of the Pennsylvanian uplift is well-preserved in the Los Cañoncitos area where Bursum and Abo beds lap onto the Proterozoic core of the uplift (Kottlowski and Stewart, 1970) and evidence of Late Paleozoic sinistral-oblique normal growth-faulting has been documented (Beck, 1993). The northern tip of the uplift was located near the present northern extent of Proterozoic outcrops where it plunges northward beneath antiformal beds of the Madera Group (Beck, 1993; de Moor et al., 2005). The locations of southern and eastern margins of the uplift, however, are poorly constrained. The eastern flank of the uplift was subsequently down-dropped by Laramide and Late Cenozoic slip on the East Joyita fault and buried (Beck and Chapin, 1994). The southern part of the Joyita Uplift lies concealed beneath the Neogene Santa Fe Group of the Socorro Basin.

The angular unconformity at the base of the Bursum Formation at Los Cañoncitos is indicative of a major pulse of late Pennsylvanian Ancestral Rocky Mountains (ARM) tectonism in the Joyita Uplift (Kottlowski and Stewart, 1970, Beck, 1993; Krainer and Lucas, 2009). Beneath the Bursum at Los Cañoncitos, Atokan through Missourian strata are anomalously thin, exhibit wedge shapes and local growth-fault relationships, and contain numerous unconformities (Kottlowski and Stewart,

1970; Siemers, 1978, 1983; Beck and Chapin, 1994), all of which are suggestive of Pennsylvanian synsedimentary deformation on the western flank of the nascent uplift.

In the Los Cañoncitos area, pebbles in the Bursum Formation consist of mostly Proterozoic lithologies with subordinate clasts derived from the Madera Group. These pebble types are consistent with the rock types exposed along the west flank of the Joyita Uplift during onlap of the Bursum Formation. In contrast, pebble compositions in Bursum deposits derived from the east flank of the Joyita Uplift are dominated by Madera Group limestone and siltstone. This suggests that extensive Madera exposures existed on the east flank of the uplift during Bursum deposition, but were obscured by east-down deformation along the East Joyita fault and subsequent burial.

On the Pedernal Uplift east of the study area, Proterozoic rocks are overlain by the Abo Formation (Broadhead and Jones, 2004). North of Carrizozo, between the Chupadera fault and the Pedernal Uplift (herein termed the Carrizozo Bench; Fig. 11), well data show the Bursum Formation is absent and the Abo Formation lies unconformably on

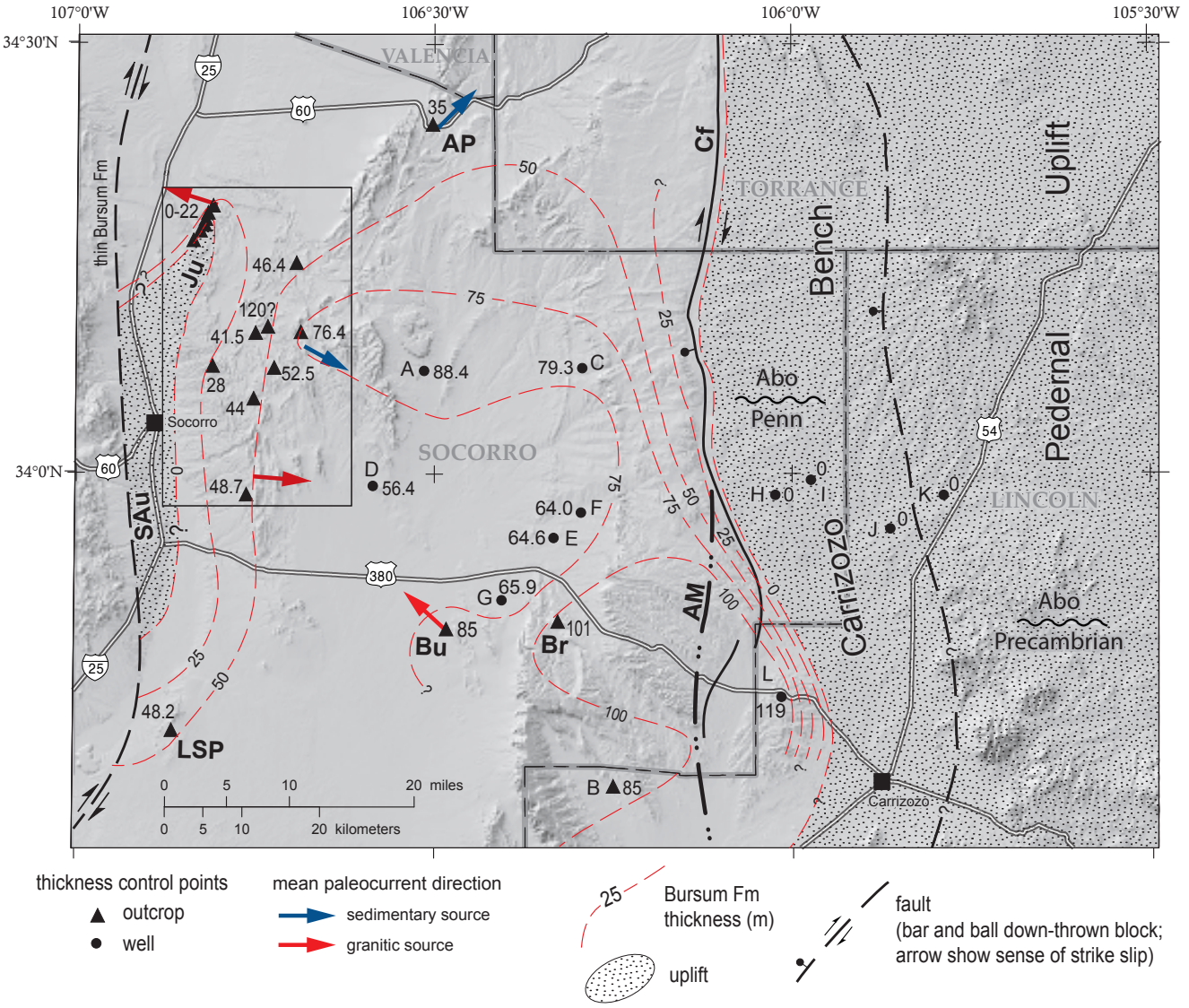

Figure 11. Digital elevation map showing modern topography of central New Mexico superimposed by latest Pennsylvanian paleogeography, major faults, mean paleocurrents, and regional Bursum thicknesses from outcrops and petroleum wells. The rectangle east of Socorro encloses area of Figures 6, 9, and 10. Paleocurrent directions within the rectangle are generalized; see Figures 4 and 6 for details. AM—aeromagnetic linear gradient which may represent lower-plate (sub-Yeso Formation) position of the Chupadera fault (Cather, 2009). AP—Abo Pass section (Bursum Formation thickness from Krainer et al., 2009; average paleocurrent direction is from Fig. 4A). B—measured section B of Bachman (1968). Bu—Bursum Formation type section (thickness and average paleocurrent direction from Lucas et al., 2002). Br—Bursum Formation thickness at the Bruton Formation type section (Bursum thickness from Lucas and Krainer, 2009). Cf—Chupadera fault. Ju—Joyita Uplift. LSP—Little San Pascual Mountain [Bursum thickness here is interpreted from the measured section of Pennsylvanian unit 4 of Geddes (1963), south of Little San Pascual Mountain. The section is too fine-grained for paleocurrent analysis.]. Penn—denotes pre-Bursum Pennsylvanian strata unconformably overlain by the Abo Formation on the Carrizozo Bench. SAu—San Antonio Uplift. Bursum Formation thicknesses in wells are from Broadhead and Jones (2004; note that these thickness estimates are based of well cuttings and geophysical logs available from the New Mexico Library of Subsurface Data at the New Mexico Bureau of Geology and Mineral Resources, and exclude wells for which only scout cards or sample logs are available): A—Skelly Oil No. 1 Goddard; C—Yates Petroleum No. 1 McCaw Federal; D—Anderson No. 1 Wishbone; E—Lockhart No. 3 Lockhart; F—Virgle Landreth No. 1 Federal; G—Sun Oil No. 1 Bingham State; H—Manzano Oil No. 1 Cathead Mesa; I—Primero No. 1 Dulce Draw State; J—Primero No. 1 Jackson Ranch Federal; K—Manzano Oil No. 1 Spaid Buckle; L—Standard Oil Co. of Texas No. 1 J.F. Heard-Federal.

older Pennsylvanian strata (Broadhead and Jones, 2004). The lacuna associated with this unconformity is best constrained by the Manzano Oil No. 1 Cathead Mesa well, where an unpublished fusulinid study by Garner Wilde (cited by Broadhead and Jones, 2004) indicates the Abo Formation unconformably overlies lower Atokan strata. The Bursum Formation and the upper part of the Pennsylvanian section are thus missing in the well (Broadhead, 2009). The Carrizozo Bench represents a structural terrace along the western flank of the Pedernal Uplift that was moderately uplifted sometime before the Abo Formation was deposited. The Chupadera fault, a southward continuation of the dextral Picuris–Pecos fault (Cather, 2009), thus experienced local east-up stratigraphic separation in the region north of Carrizozo during the Late Pennsylvanian and/or earliest Permian.

The nature and location of faults that controlled deformation during the Pennsylvanian in central New Mexico are poorly known, largely because of overprinting by the subsequent Laramide and rift deformations. The best documented Pennsylvanian faults lie along the west flank of the Joyita Uplift, where normal faults with west and northwest strikes are present. A particularly well-preserved fault there was active as a steep, north-striking,

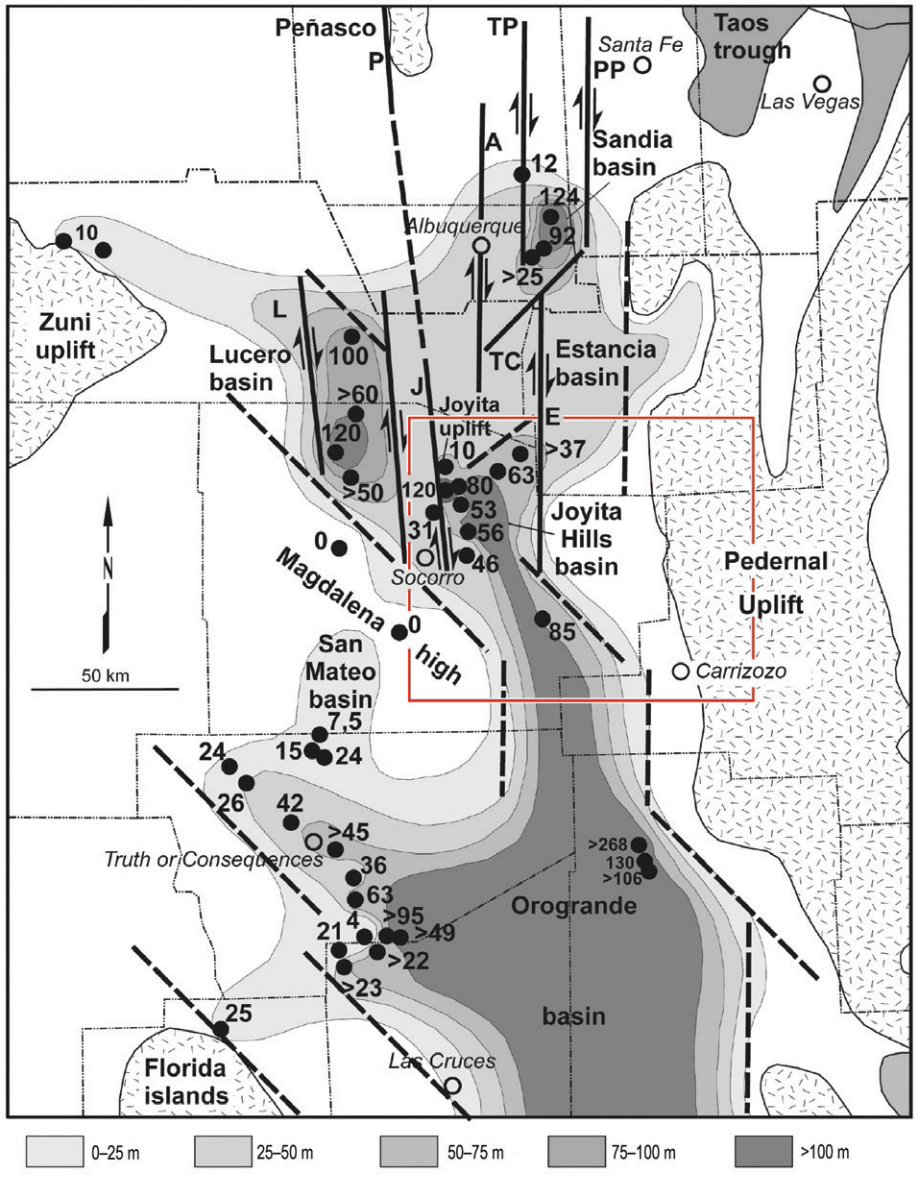

Figure 12. Isopach map of the Bursum Formation and equivalent units in central and northern New Mexico (Krainer and Lucas, 2009), showing paleogeographic features (including the "Joyita Hills Basin"), thickness control points (dots, with thicknesses in meters), and the area of Figure 11 (red rectangle). Note that this map does not consider the Bursum thicknesses documented in the subsurface by Broadhead (1997) and Broadhead and Jones (2004). Heavy lines are faults inferred by Krainer and Lucas (2009), several of which are incorrectly located or are hypothetical (i.e., they do not correspond to known faults or geophysical lineaments; see comments for individual faults in brackets). Faults are: P—Peñasco fault [This is the Nacimiento fault of most workers.]; A—Albuquerque fault [Does not correspond to any known, single fault.]; TP—Tusas–Picuris fault [This fault is depicted ~40 km too far to the west. It actually passes north-south through Santa Fe (see Cather et al., 2006).]; PP—Picuris–Pecos fault [This fault is depicted ~30 km too far west. The actual fault lies ~15 km east of Santa Fe where it forms the western margin of the Taos Trough.]; L—Lucero fault [hypothetical]; J— Joyita fault [This presumably is the West Joyita fault, a rift fault with no known Paleozoic precursor. Its southward projection through the Bursum exposures in the Quebradas region is incorrect.]; TC—Tijeras–Cañoncito fault [Only the southwestern part of this fault is depicted.]; E—Estancia fault [Hypothetical, except in its northern part where it corresponds approximately to the Montosa fault.].

left-oblique normal fault during the latest Pennsylvanian (Beck and Chapin, 1991; Beck, 1993; Beck and Chapin, 1994). The Polvadera thrust fault in the Lemitar Mountains ~15 km northwest of Socorro records north-south shortening during Atokan time (Chamberlin, 1983; Chamberlin et al., 2001; Chamberlin, 2004). The Chupadera fault (termed the Monte Prieto–Liberty Hill structural zone by Broadhead and Jones, 2004) described above is the only other fault in the region for which Pennsylvanian slip can be reasonably inferred, although many other faults must have been active during that time. On Figure 11 a dextral fault, corresponding to the modern Socorro Canyon fault, is depicted along the west flank of the San Antonio Uplift. Pennsylvanian slip on this fault is speculative, and is shown only to suggest the possibility that the San Antonio Uplift might be analogous to the dextral transpressive Laramide Sierra Uplift (Cather, 2009) in the same location.

Two diametrically opposed models for regional faulting during the Pennsylvanian have been proposed. Beck (1993) and Beck and Chapin (1994) proposed a sinistral transtensional model for ARM deformation in New Mexico, and Krainer and Lucas (2009, their fig. 7, reproduced here as Fig. 12) presented a dextral transpressional model. Evidence is scant but probably favors the dextral model (see summary of ARM slip-sense indicators in Cather et al., 2006). It should be noted, however, that several of the ARM faults depicted in the dextral model of Krainer and Lucas (2009) are hypothetical (i.e., they correspond to no known fault or geophysical feature) or are incorrectly located (see caption of Fig. 12).

Krainer and Lucas (2009) interpreted the Bursum Formation southeast of the Joyita Uplift to have been deposited within a narrow (~35 km wide), symmetric, north-northwest-trending basin, which they termed the Joyita Hills Basin. Their isopach map (Fig. 12) depicts a narrow zone (~10 km wide) of thick (>100 m) Bursum Formation in east-central Socorro County that defines the axis of the basin. The only control point that supports such a thickness, however, is the questionable 120 m thickness measured by Krainer and Lucas (2009) in their Gallina Well section. Even if the 120 m thickness is correct, the Gallina Well section is surrounded by measured sections in which the Bursum Formation is relatively thin (Fig. 6). The extension of a zone of thick (>100 m) Bursum far to the south-southeast of Gallina Well by Krainer and Lucas (2009) is thus unlikely, if standard contouring protocols are observed.

The eastern side of the Joyita Hills Basin of Krainer and Lucas (2009) is demarcated by purported zero thickness of the Bursum Formation in east-central Socorro County. No evidence for missing Bursum in this area, however, was presented by them. Contrary to the interpretations of Krainer and Lucas (2009), significant Bursum thicknesses (56.4–119 m) have been documented in petroleum exploration wells of eastern Socorro County and western Lincoln County (Fig. 11) by Broadhead and Jones (2004).

There is no evidence for a narrow, elongate basin of Bursum age extending south-southeast from the Joyita Uplift, as was depicted by Krainer and Lucas (2009; their Joyita Hills Basin). Instead, a broad area (as much as 100 km wide) of gradually southeastward-thickening Bursum deposits existed between the Joyita Uplift and the vicinity of Carrizozo. I regard the area of Bursum deposition east of the Joyita and San Antonio uplifts as simply a weakly subsided saddle-shaped platform between the deeper Orogrande Basin and Estancia basins, the latter of which contains as much as 335 m of Bursum Formation within the deep Perro sub-basin (Broadhead, 1997). I suggest that the incorrectly characterized term "Joyita Hills Basin" be abandoned.

Summary

Because the Bursum Formation is widely distributed and relatively coarse-grained, it is perhaps the most suitable Upper Paleozoic unit in central New Mexico for paleocurrent analysis. Such analyses are the best source of paleoslope information, which in turn allows for a better determination of paleogeography. Paleocurrent data from the Bursum Formation in the Quebradas region east of Socorro indicate the presence of major Proterozoic exposures on a Late Pennsylvanian highland, herein termed the San Antonio Uplift, in what is now the southern part of the Socorro Basin. Isopach trends, isolith maps of percent marine strata, and maximum clast-size distribution in the Bursum all support such an interpretation.

The San Antonio Uplift and the long-known Joyita Uplift formed the western margin of a broad, weakly subsided shelf on which gradually southeast-thickening Bursum deposits accumulated. North of Carrizozo, the Chupadera fault marked the eastern limit of Bursum deposition. Between the Chupadera fault and the Pedernal Uplift to the east, a terrace of moderate structural relief (the Carrizozo Bench) was the site of erosion sometime prior to deposition of the Abo Formation.

Acknowledgments

Field work was supported by the New Mexico Bureau of Geology and Mineral Resources and by STATEMAP contracts awarded to the Bureau. I have benefited from many useful conversations concerning the Bursum Formation with Ron Broadhead, Bob Colpitts, Richard Chamberlin, Bruce Allen, Dave Love, and Spencer Lucas. Leo Gabaldon, Stephanie Chavez, and Mark Mansell created the figures. I thank Sevilleta National Wildlife Refuge for access to refuge lands. An early draft of the paper was improved by reviews from Ron Broadhead and Richard Chamberlin. The paper was further improved by comments from NMG editor Bruce Allen and two anonymous reviewers.

References

Allen, B.D., Love, D.W., and McCraw, D.J., 2013, Uppermost Pennsylvanian Bursum Formation near Cibola Spring, Sevilleta National Wildlife Refuge, Socorro County, New Mexico: New Mexico Museum of Natural History and Science, Bulletin 59, p. 233–238.

Altares, T., III, 1990, Stratigraphic description and paleoenvironments of the Bursum Formation, Socorro County, New Mexico [M.S. thesis]: Socorro, New Mexico Institute of Mining and Technology, 184 p.

Arendt, W.W., 1971, The geology of the Joyita Hills, Socorro County, N.M. [M.S. thesis]: Albuquerque, The University of New Mexico, 75 p.

Bachman, G.O., 1968, Geology of the Mockingbird Gap quadrangle, Lincoln and Socorro counties, New Mexico: U.S. Geological Survey, Professional Paper 594-J, 43 pp.

Beck, W.C., 1993, Structural evolution of the Joyita Hills, Socorro County, New Mexico [Ph.D. dissertation]: Socorro, New Mexico Institute of Mining and Technology, 187 p.

Beck, W.C., and Chapin, C.E., 1991, Structural data from the Joyita uplift: Implications for ancestral Rocky Mountain deformation within central and southern New Mexico: New Mexico Geological Society, Guidebook 42, p. 183–190.

Beck, W.C., and Chapin, C.E., 1994, Structural and tectonic evolution of the Joyita Hills, central New Mexico; implications of basement control on Rio Grande Rift, *in* Keller, G.R., and Cather, S.M., eds., Basins of the Rio Grande Rift: Structure, Stratigraphy, and Tectonic Setting: Geological Society of America Special Paper 291, p. 187–205.

Broadhead, R.F., 1997, Subsurface and petroleum geology of Estancia Basin, New Mexico: New Mexico Bureau of Mines and Mineral Resources, Bulletin 157, 54 pp.

Broadhead, R.F., 2009, Oil, natural gas and helium potential of the Chupadera Mesa area, Lincoln and Socorro counties, New Mexico: New Mexico Geological Society, Guidebook 60, p. 359–374.

Broadhead, R.F., and Jones, G., 2004, Oil, natural gas, and helium potential of the Chupadera Mesa area, Lincoln and Socorro counties, New Mexico: New Mexico Bureau of Geology and Mineral Resources, Open-file Report 478, CD ROM.

Cather, S.M., 2002 (revised 2016), Geologic map of the San Antonio quadrangle, Socorro County, New Mexico: New Mexico Bureau of Geology and Mineral Resources, Open-file Geologic Map 58, scale 1:24,000.

Cather, S.M., 2009, Tectonics of the Chupadera Mesa region, central New Mexico: New Mexico Geological Society, Guidebook 60, p.127–137.

Cather, S.M., and Colpitts, R.M., Jr., 2005 (revised 2016), Geologic map of the Loma de las Cañas quadrangle, Socorro County, New Mexico: New Mexico Bureau of Geology and Mineral Resources, Open-file Geologic Map 110, scale 1:24,000.

Cather, S.M., Colpitts, R.M., Jr., and Hook, S.C., 2004 (revised 2016), Geologic map of the Mesa del Yeso quadrangle, Socorro County, New Mexico: New Mexico Bureau of Geology and Mineral Resources, Open-file Geologic Map 92, scale 1:24,000.

Cather, S.M., Karlstrom, K.E., Timmons, J.M., and Heizler, M.T., 2006, Palispastic reconstruction of Proterozoic basement-related aeromagnetic features in north-central New Mexico: Implications for Mesoproterozoic to Late Cenozoic tectonism: Geosphere, v. 2, p. 299–323.

Cather, S.M., Osburn, G.R. and Hook, S.C., 2007 (revised 2016), Geologic map of the Cañon Agua Buena quadrangle, Socorro County, New Mexico: New Mexico Bureau of Geology and Mineral Resources, Open-file Geologic Map 146, scale 1:24,000.

Cather, S.M., Colpitts, R.M., Jr., Green M., Axen, G.A., and Flores, S., 2012 (revised 2016), Geologic map of the Sierra de la Cruz quadrangle, Socorro County, New Mexico: New Mexico Bureau of Geology and Mineral Resources, Open-file Geologic Map 227, scale 1:24,000.

Cather, S.M., Osburn, G.R., McIntosh, W.C., Hook, S.C., Flores, S., and Green, M., 2014 (revised 2016), Geologic map of the Bustos Well quadrangle, Socorro County, New Mexico: New Mexico Bureau of Geology and Mineral Resources, Open-file Geologic Map 237, scale 1:24,000.

Chamberlin, R.M., 1983, Cenozoic domino-style crustal extension in the Lemitar Mountains, New Mexico: A summary: New Mexico Geological Society, Guidebook 34, p. 111–118

Chamberlin, R.M., 2004, Preliminary geologic map of the San Lorenzo Springs quadrangle, Socorro County, New Mexico: New Mexico Bureau of Geology and Mineral Resources, Open-file Geologic Map 86, scale 1:24,000.

Chamberlin, R.M., Cather, S.M., Nyman, M.T., and McLemore, V.T., 2001, Geologic map of the Lemitar quadrangle, Socorro County, New Mexico: New Mexico Bureau of Geology and Mineral Resources, Open-file Geologic Map 38, scale 1:24,000.

Colpitts, R.M., Jr., 1986, Geology of the Sierra de la Cruz area, Socorro County, New Mexico [M.S. thesis]: Socorro, New Mexico Institute of Mining and Technology, 166 p.

Davydov, V.I., Glenister, B.F., Sinosa, C., Ritter, S.M., Chernykh, V.V., Wardlaw, B.R. and Snyder, W.S., 1998, Proposal of Aidaralash as Global Stratotype Section and Point (GSSP) for base of the Permian System: Episodes, v. 21, p. 11–17.

de Moor, M., Zinsser, A., Karlstrom, K., Chamberlin, R., Connell, S. and Read, A., 2005, Preliminary geologic map of the La Joya 7.5-minute quadrangle, Socorro County, New Mexico: New Mexico Bureau of Geology and Mineral Resources, Open-File Geologic Map OF-GM 102, scale 1:24,000, 1 sheet.

Fagrelius, K.H., 1982, Geology of the Cerro del Viboro area, Socorro County, New Mexico [M.S. thesis]: Socorro, New Mexico Institute of Mining and Technology, 135 p.

Geddes, R.W., 1963, Structural geology of Little San Pasqual Mountain and adjacent Rio Grande trough [M.S. thesis]: Socorro, New Mexico Institute of Mining and Technology, 64 p.

Kottlowski, F.E., and Stewart, W.J., 1970, The Wolfcampian Joyita uplift of central New Mexico: New Mexico Bureau of Mines and Mineral Resources, Memoir 23, p. 3–31.

Krainer, K. and Lucas, S.G., 2009, Cyclic sedimentation of the Upper Pennsylvanian (lower Wolfcampian) Bursum Formation, central New Mexico: Tectonics versus glacioeustasy: New Mexico Geological Society, Guidebook 60, p. 167–182.

Krainer, K. and Lucas, S.G., 2013, The Pennsylvanian–Permian Bursum Formation in central New Mexico: New Mexico Museum of Natural History and Science, Bulletin 59, p. 143–160.

Krainer, K., Lucas, S.G., and Vachard, D., 2009, The Upper Carboniferous Bursum Formation at Abo Pass, Socorro County, New Mexico: New Mexico Geological Society, Guidebook 60, p. 98–102.

Lucas, S.G. and Krainer, K., 2004, The Red Tanks Member of the Bursum Formation in the Lucero uplift and regional stratigraphy of the Bursum Formation in New Mexico: New Mexico Museum of Natural History and Science, Bulletin 25, p. 43–52.

Lucas, S.G. and Krainer, K., 2009, Pennsylvanian stratigraphy in the northern Oscura Mountains, Socorro County, New Mexico: New Mexico Geological Society, Guidebook 60, p. 153–165.

Lucas, S.G., Barrick, J.E., Krainer, K., and Schneider, J.W., 2016, Pennsylvanian-Permian boundary at Carrizo Arroyo, central New Mexico: New Mexico Geological Society, Guidebook 67, p. 303–311.

Maulsby, J., 1981, Geology of the Rancho de Lopez area east of Socorro, New Mexico [M.S. thesis]: Socorro, New Mexico Institute of Mining and Technology, 85 p.

Montañez. I.P., and Poulsen, C.J., 2013, The Late Paleozoic ice age: An evolving paradigm: Annual Reviews of Earth and Planetary Sciences, v. 41, p. 629–656.

New Mexico Bureau of Geology and Mineral Resources, 2003, Geologic Map of New Mexico, scale 1:500,000, two sheets.

Siemers, W.T., 1978, The stratigraphy, petrology, and paleoenvironments of Pennsylvanian rocks in west-central New Mexico [Ph.D. dissertation]: Socorro, New Mexico Institute of Mining and Technology, 275 p.

Siemers, W.T., 1983, The Pennsylvanian System, Socorro region, New Mexico: Stratigraphy, petrology, depositional environments: New Mexico Geological Society, Guidebook 34, p. 147–755.

Rejas, A., 1965, Geology of the Cerros de Amado area, Socorro County, New Mexico [M.S. thesis]: Socorro, New Mexico Institute of Mining and Technology, 128 p.

Weissmann, G.S., Hartley, A.J., Nichols, G.J., Scuderi, L.A., Olson, M., Buehler, H., Banteah, R., 2010, Fluvial form in modern continental sedimentary basins: Distributive fluvial systems: Geology, v. 38, p. 39–42.

Wilpolt, R.H., MacAlpin, A.J., Bates, R.I. and Vorbe, G., 1946, Geologic map and stratigraphic sections of Paleozoic rocks of Joyita Hills, Los Pinos Mountains, and northern Chupadera Mesa, Valencia, Torrance, and Socorro Counties, New Mexico: U.S. Geological Survey, Oil and Gas Investigations Preliminary Map 61, scale 1:63,360.

Reassessment of features in the Aden Crater lava flows, Doña Ana County, New Mexico

René A. De Hon and *Richard A. Earl*
Department of Geography, Texas State University, 601 University Drive, San Marcos, Texas 78666

Abstract

Aden Crater lava field, encompassing 75 km^2 in south-central New Mexico, offers excellent examples of features of basalt flows associated with a shield volcano. Aerial images and recent field examination allow a re-evaluation of the lava field's surface features. Aden Crater sits atop the summit of the shield (referred to herein as the cone) which is surfaced by channeled lavas merging downslope into lobate lava flows. The cone and its adjacent flow field are divided into five facies. Extending away from the cone are several features associated with inflation and collapse processes, representing early-formed tumuli that did not develop as completely as those farther downslope.

Introduction

The Aden Crater lava field encompassing 75 km^2 in south-central New Mexico offers excellent examples of features of basalt flows associated with an Icelandic-type shield volcano. In this paper, we present interpretations of some of these features based on recently published work (Walker, 2009), new aerial images, and field examination of the flows conducted in 2012 and 2014. Specifically, we identify four flow facies that formed as a function of the rheology of lava during flow emplacement. We examine the mechanisms of pit formation on the flows, and revisit the relationship of pits to faults in the region.

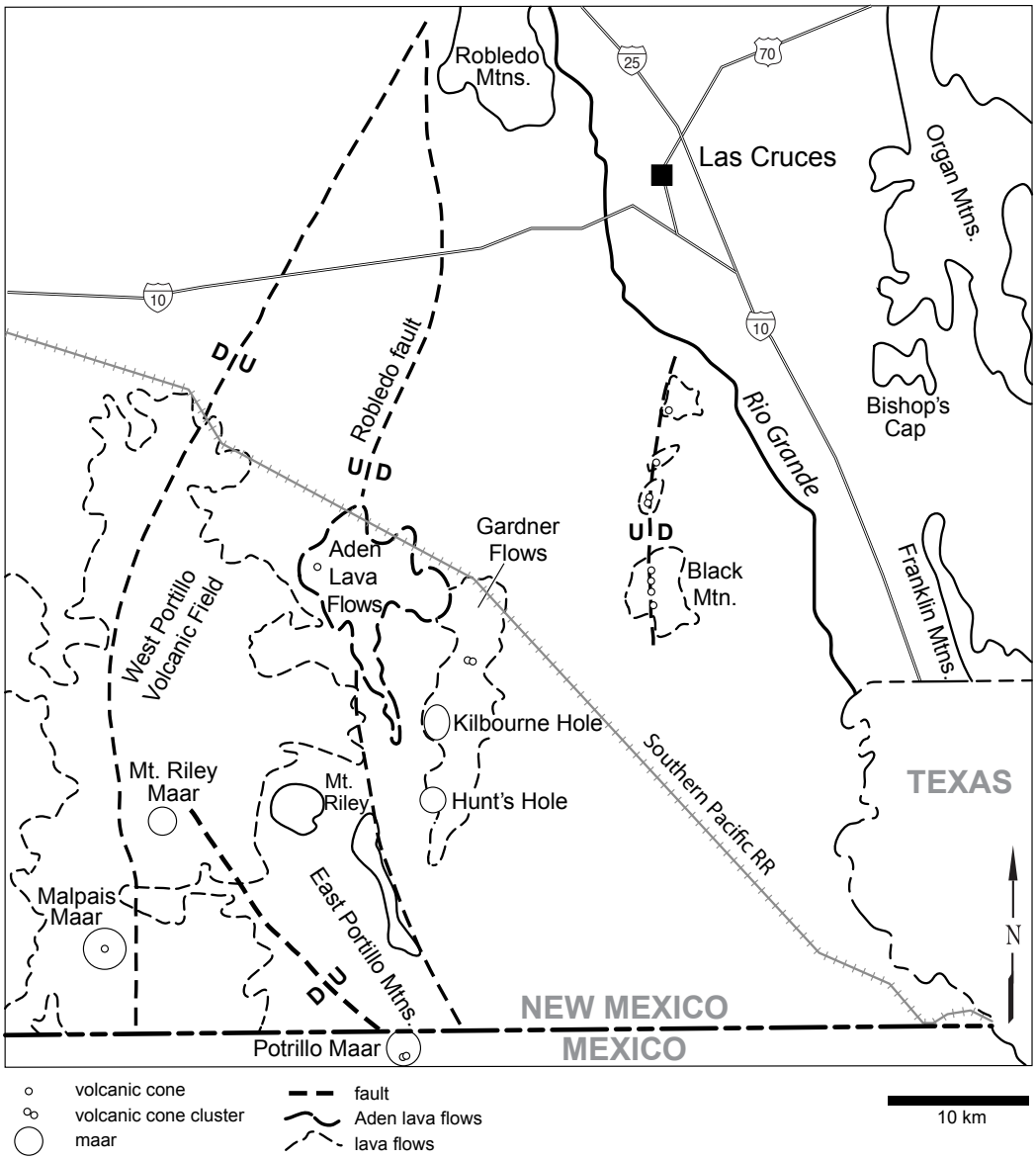

Figure 1. Location of Aden lava flows in south-central New Mexico. Cenozoic basaltic volcanic features in the area include cinder cones, maars, and the Aden shield.

Regional setting

Located approximately 40 km southwest of Las Cruces in Doña Ana County, New Mexico, Aden Crater and its associated flows are the youngest volcanic features in a diverse, monogenetic basalt field known as the Potrillo Volcanic Field (Fig. 1). The Potrillo Volcanic Field (PVF) occupies the southernmost part of the Rio Grande rift, where it merges with the New Mexico portion of the Basin and Range Province (Seager and Morgan, 1979). The PVF is included in the Organ Mountain-Desert Peaks National Monument established in 2014 and is accessible by unpaved county roads.

The Aden flows overlie the La Mesa geomorphic surface, with an age of ca. 0.6 Ma, which marks the aggradational top of ancestral Rio Grande deposits of the Camp Rice Formation and is characterized by well-developed aridisol soils with Cca/K horizons approximately 50–200 cm thick (Bulloch and Neher, 1980; Seager et al., 1984; Mack et al. 2006). The region is in the northern Chihuahuan desert and presently has an arid climate with a summer precipitation maximum. The native desert scrub vegetation includes creosote, mesquite and yucca as dominant species. Eolian sand deposits within topographic lows in and around the flows are commonly covered by buffalo gourd.

Dating of the Aden shield and flows is problematic. Seager et al. (1984) reported a K-Ar age from lava-lake basalt inside the Aden crater of 0.53 Ma, whereas ^{3}He surface-exposure dating has yielded ages ranging from 18.3–15.7 ka (Anthony and Poths, 1992) to 22 ka (Williams and Poths, 1994). We consider the younger ages more realistic based qualitatively on the degree of weathering of Aden volcanic features. For example, a spatter cone is present within the crater that retains delicate features and surface textures associated with accumulation of the ejected spatter, which might be expected to be considerably more weathered (both chemically and physically) if exposed to five full glacial episodes and extended periods of significantly cooler and wetter climate (e.g., Betancourt et al., 2001; Barbante et al., 2010).

Volcanic activity in the PVF covers 1,040 km^2 including the 1,800 m high Mt. Riley, which consists of a Tertiary rhyodacite stock, volcaniclastic sedimentary deposits and Quaternary basaltic volcanic rocks (Hoffer, 1976a). The western part of the PVF (West Potrillo Mountains) covers an area of 590 km^2. It includes more than 100 cinder cones averaging 60 to 150 m in height, with surface-exposure ages ranging from 80 to 17 ka (Anthony and Poths, 1992; Thompson et al., 2005). The basalt flows of Aden stand in sharp contrast to the cinder cones of the West Potrillo Mountains or the explosive activity that formed the maar craters to the south of Aden.

There are at least five maar-type craters in the PVF. Kilbourne Hole, Hunt's Hole, and the Potrillo maar lie on the east side of the field (De Hon 1965a, Reeves and De Hon, 1965, Hoffer, 2001, Padovani and Reid, 1989). Riley maar (Bersch, 1977) is located in the interior of the West Potrillo field, and the Malpais maar (Page, 1975), near the south end of the field, is almost completely buried beneath a 75-m-high cone that was built on its floor.

The Gardner craters complex is a cluster of cinder cones to the east-southeast of the Aden flows that is associated with the 80 km^2 Afton lava field that includes Kilbourne and Hunt's Holes and extends 4 km north and 13 km south of the Gardner cinder cones. The Afton basalt is partially obscured by eolian sand cover and low scrub brush. It is best exposed in its northern reaches near the Afton railroad crossing and in vertical sections up to 3 m thick in Kilbourne and Hunt's Holes. The Afton flows, dated at 72–81 Ka by K-Ar (Seager et al. 1984), are overlain by the Aden flows northwest of the Gardner cinder cones.

Additional cinder cones and associated flows are present in a north-south chain 25 km to the east of Aden (Fig. 1). The Santo Tomas-Black Mountain basalts were erupted from four centers. Six lava flows are present at Black Mountain, three at Santo Tomas, and one each at Little Black Mountain and San Miguel. The basalts are in the 69–77 Ka age range by K-Ar dating (Seager et al.,1984).

Structural setting

La Mesa is an aggraded surface of ancestral Rio Grande sediments that accumulated in the Mesilla Basin, one of several fault-bounded basins along the Rio Grande rift (Hawley, 1981). Except for faults related to uplift of the East Potrillo Mountains (Fig. 1), which exhibit visible scarps, faults on the La Mesa surface were originally inferred based in part on an apparent alignment of volcanic features (Kilburn et al., 1988). Fault traces are now documented using well-log analysis and geophysical methods (e.g., Seager et al. 1987). The Robledo—East Potrillo fault exhibits a 100 m down to the east offset and cuts across the La Mesa surface beneath the Aden basalts and extends to the vicinity of Potrillo maar. This range-bounding normal fault on the east side of the East Potrillo Mountains offsets pyroclastic surge deposits associated with the Potrillo maar (Seager and Mack, 1994). Alignment of 12 cinder cones in the Black Mountain-Santo Tomas chain and an 11 km-long series of depressions south of the volcanic chain coincide with a down to the east fault with approximately 170 m of offset in the subsurface (Seager and Mack, 1994). The alignment of various pits on the flanks of the Aden shield were presumed to be formed by venting along the trace of the Robledo fault beneath the flows (De Hon, 1965b: Hoffer, 1976a, b). It was also thought that the Gardner cone complex and Kilbourne and Hunt's Holes were aligned along the hypothetical Fitzgerald fault (De Hon, 1965a; Hoffer, 1976a, b). Subsurface evidence (Seager et al. 1987) and additional observations, developed in following sections in this paper, no longer support the existence of the Fitzgerald fault.

Aden cone

The Aden shield volcano (Figs. 1, 2) is a relatively young feature of the Portillo Volcanic Field. A nontechnical description of the Aden crater was published by Perkins (1949). De Hon (1965b) and Hoffer (1975a, 1990) also described the crater's features, and Kahn (1987) conducted a more extensive study. In this paper Aden "cone" is used refer to the summit area of the shield volcano, which includes Aden crater and the comparatively steep slopes surrounding the crater. The Aden cone is 2.5 km in diameter (Fig. 3) and rises 50 m above the surrounding landscape. Aden crater (unit cr of Fig. 3) is a broad, shallow depression, 350 m in diameter, on top of the cone. The crater rim consists of a steep pile of agglutinate, 2.5 to 3.5 m high, built of spatter from a lava lake that occupied the crater. Open tension fissures ring the crater floor inside the rim. A small 3 m high spatter cone near the center of the crater rises above the lake lavas, and a 120 m diameter, 20 m deep pit is present in the southern part of the crater.

Figure 2. The Aden shield viewed from the north. The gentle slopes lead up to a relatively steep rampart of spatter lava.

Figure 3. Annotated aerial photograph of a portion of the Aden basalt field. The topographically high summit of the shield referred to herein as the Aden cone is built on a basal unit of scabby lava flows (unit sc). The lower flanks of the cone consist of a lobate flow (unit lo), upper channeled flows (unit ch), and the broad, apical crater (unit cr). The early scabby flows were thin fluid flows. Several features are present approximately midway downslope on the scabby flows that represent local tumescence on thin-skinned flow material—including collapse pits (unit cp), rootless shields (unit rs), and blocky rimmed pits (unit br). The bulk of the lava field beyond the cone is shown here as inflated flows (unit if). Inflation pits (unit ip) are present on inflated flows. North is toward the top of the photo; UTM coordinates for the center of the crater are: 305707E, 3549925N, zone 13 (horizontal datum NAD83).

Guano mining from a fumarole on the southeast rim uncovered a well-preserved skeleton of an extinct giant ground sloth, with two associated radiocarbon ages of 9,840 ±160 and 11,080 ±200 BP (Lull, 1929; Simons and Alexander, 1964). The fumarole is approximately 5 ft. (1.5 m) in diameter at the surface and descends vertically for 65 ft. (19.8 m) before becoming an inclined tube extending 80 ft. (24.4 m) to the chamber that contained the guano and sloth remains.

The extent of the lava flows associated with the Aden shield were mapped by Seager et al. (1987). The Aden flows are alkaline olivine basalt and basanite (Kahn 1987; Hoffer, 2001). If the ^{3}He surface-exposure dating of Anthony and Poths (1992) is accurate, the Aden flows at 18.2–15.7 Ka are the youngest in the PVF.

Updated interpretation of flows and features

We have divided the Aden cone and associated proximal flows into three facies (units ch, lo, and sc in Fig. 3) based on surface physiography and mode of emplacement. The cone consists of an upper channeled flow facies (unit ch) that passes downslope into a lobate flow facies (unit lo). The channeled flow facies was formed by lavas spilling over the crater rim from the lava lake; it consists of levied lava channels and lava tubes 0.5–1.5 m wide on slopes of 8 to 15 percent (4.6 to 8.5 degrees). The channels branch in a distributary pattern downslope. The breaching of lava levies to form distributary channels is responsible for the horseshoe-shaped lava ridges, *herradura,* described by Hoffer (1971). Flows emerging from the channels spread as overlapping lobate flows as the slopes decrease to 3–5 percent (1.7–2.9 degrees) at lower elevations. The lobate flows (unit lo) overlie thin flows on the outer flanks that are characterized by a scabby flow facies (unit sc) consisting of intercalated, thin, pahoehoe flows with local micro-relief of 0.5 m that makes up the base of the cone. The scabby flow facies represents the first, very fluid flows that issued from the vent. As lava spread away from the vent, it cooled, viscosity increased, and the flows thickened by inflation. In the distal flow field, individual flows exhibit varying degrees of inflation (unit if in Fig. 3).

Flow field

The thin flows at lower elevations (units sc and if, Fig. 3) are partially obscured by an eolian sand cover, scrub vegetation, and grasses. The higher elevations are generally free of cover and much fresher in appearance. Depressions in the flows and swales between adjacent flow margins are generally floored by sand which supports a hardy growth of buffalo gourd.

Figure 4. Inflation pits (ip) are formed where thin flows surrounded local rises on the pre-flow surface. The flows inflated around the rise leaving a depression. The thickest flows form flat-topped, inflation plateaus (if), which develop peripheral fissures (pf) and steep flow margins. Less inflated flows form pressure ridges and flat-topped plateaus with rounded margins. The surface of the inflated flows have rectilinear joint sets with 5–10 m spacing. North is toward the top of the photo; area shown is located in the distal flow field, 3.5 km east of the center of the crater.

The Aden flow field consists of relatively thick, flat-surfaced flows intermingled with thinner flows. The thicker flows form by the process of inflation as described by Walker (1991, 2009) in Hawaii. Inflation occurs when fluid lavas begin to develop a brittle crust underlain by a ductile core. Once the crust becomes thick enough at the flow front to impede the flow, the fluid interior begins to exert pressure, which lifts the upper surface to produce tumuli and inflation plateaus (Walker, 1991, 2009; Hon et al., 1994). Partially inflated flows with rounded margins are 1 to 3 m thick. As the crust strengthens further, flows form well-developed, flat-topped inflation plateaus with the greatest height and prominent peripheral fissures (Fig. 4).

Flat-surfaced uplifts formed by injection of lava under a surface crust have been termed "lava rises" by Walker (1991); inflated sheet lobes (Hon et al., 1994; Self et al., 1998); pressure plateaus (Wentworth and Macdonald, 1953): and inflation plateaus (Keszthelyi et al., 2004; Zimbelman et al., 2011). Fully formed inflation plateaus in the Aden field range from 100 to 300 m in width and 300 to 1,200 m in length, and reach a thickness of 4 to 5 m. The upper surfaces of the plateaus are level and cut by intersecting extension joints. The flow margin is steep, often blocky, and the edges of the inflation plateaus are marked by deep fissures. The bulk of the Aden flow field consists of the inflated flow facies (unit if in Fig. 3) which consists of overlapping flows displaying different degrees of inflation.

Pits

Various depressions associated with the Aden flows have been misinterpreted by earlier investigators (De Hon, 1965b; Hoffer, 1975b). Large, deep pits on the inflation plateaus were thought to be collapse depressions formed by withdrawal of underlying lava, and pits surrounded by raised blocky rims were thought to be explosion craters. Walker's (2009 and 1991) analysis of flow structures in Hawaii have provided analogs for the pits observed at Aden. Our re-examination of the pits on the Aden flow field recognizes four types—lava rise pits (Walker, 1991), also termed inflation pits (Scheidt et al., 2014) on the inflated plateaus, shallow collapse depressions, pits on rootless shields, and blocky rimmed depressions.

Inflated flows are pocked with large depressions ranging from 20 to 150 m across and 4 to 5 m deep. These *inflation pits* (unit ip on Figs. 3 and 4) formed in areas in which small rises in the underlying land

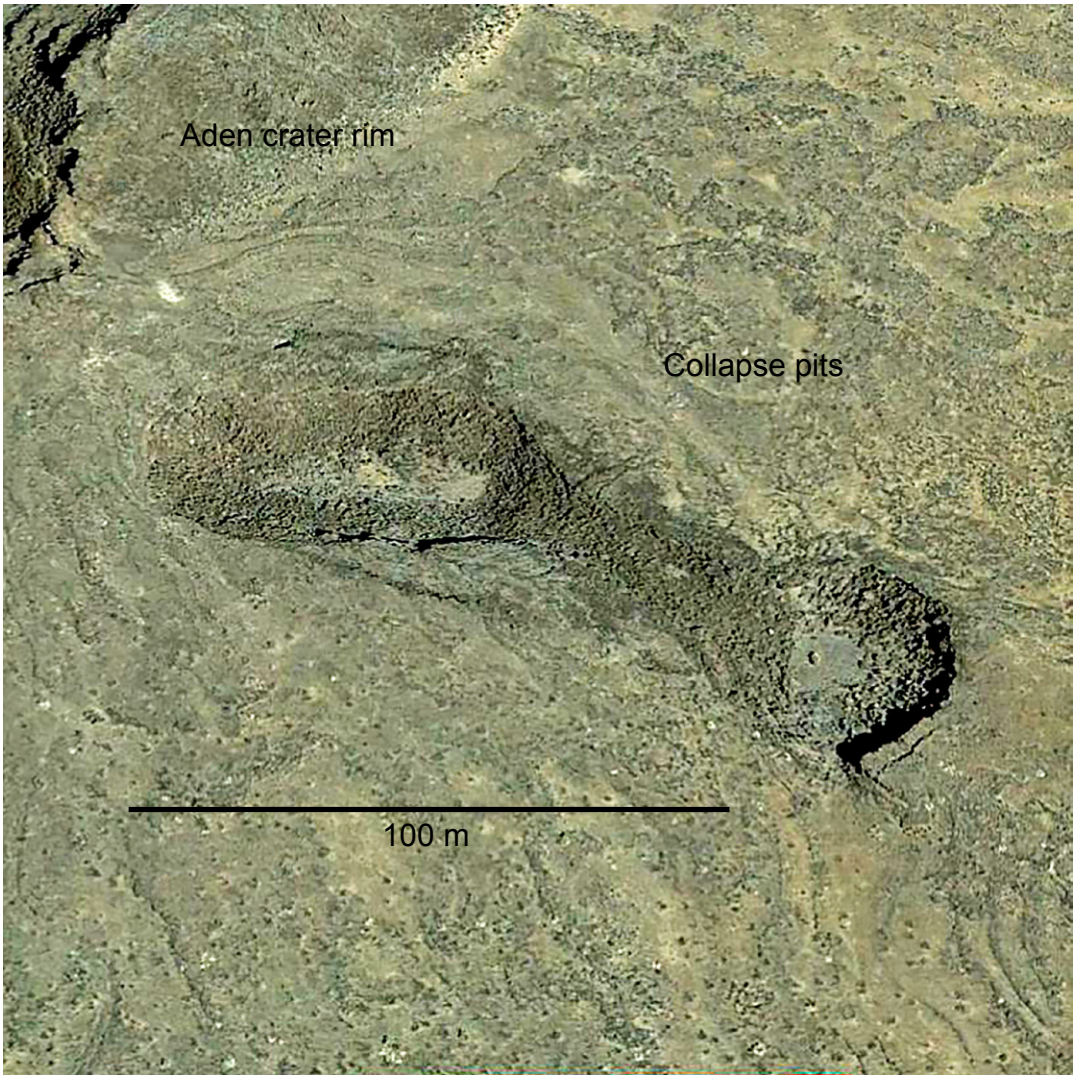

Figure 5. Collapse pits on SE flank of the Aden cone (see Fig. 3), formed by removal of lava from beneath a weak surface crust. The resulting pits are rimless and have blocky interiors.

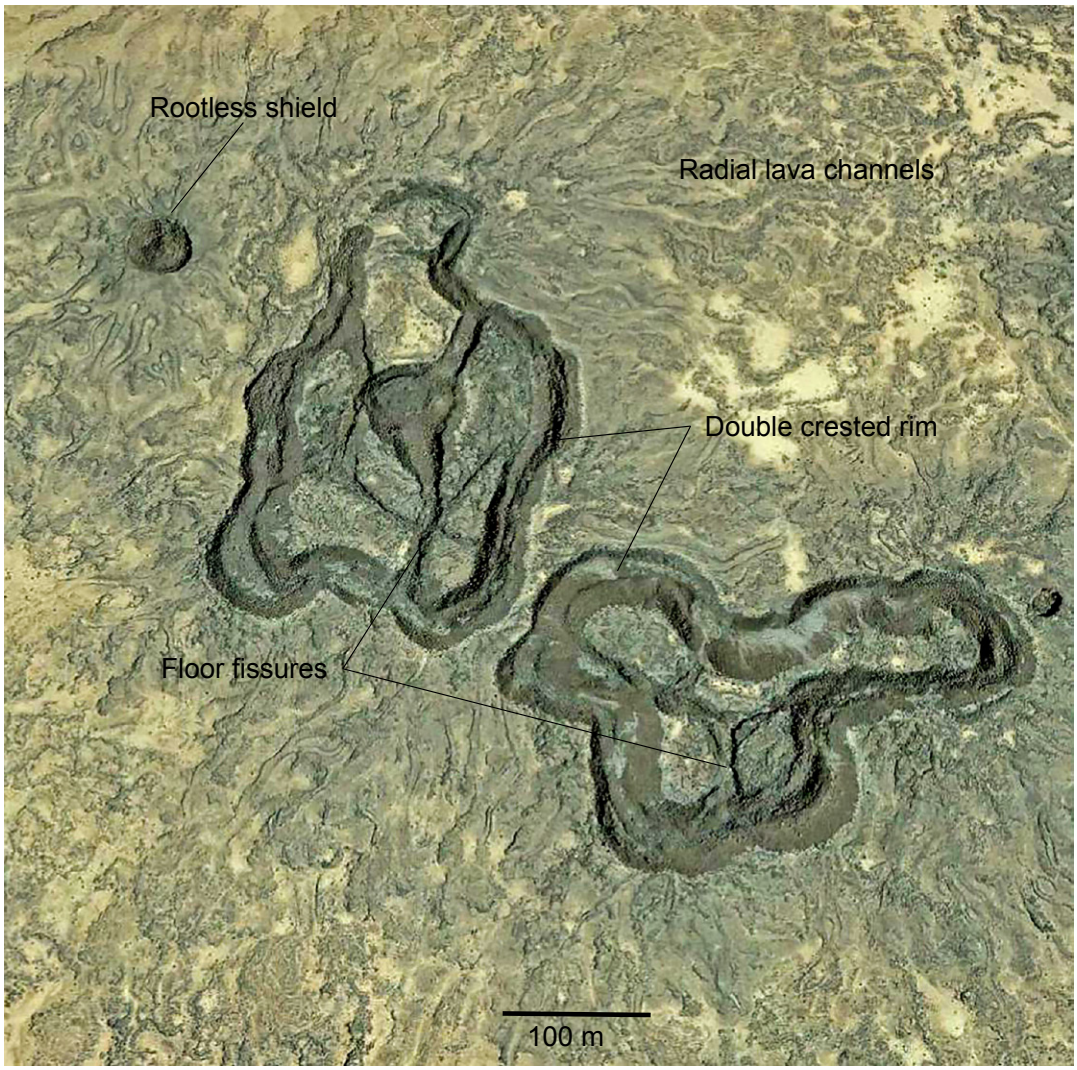

Figure 6. The scabby flow facies contains several morphologies that represent failed attempts to inflate, including rootless shields and blocky rimmed pits. Blocky rimmed depressions are irregular in plan view and represent collapsed inflation plateaus. The raised double-crested rims are split by a medial trough, and the interior "floor" is crossed by large fissures. Lava channels radiate away from the failed plateau. North is toward the top of the photo; area shown is one km southeast of the crater in Fig. 3.

surface were not covered by active flows. After a flow stopped advancing, it inflated around these patches, creating depressions on the inflated flow surface that are as deep as the flow is thick. The depressions are floored with either pre-basalt Camp Rice Formation, or thin earlier flows.

Simple *collapse pits* (unit cp on Fig. 3) result from removal of lava beneath a thin, solidified crust. The crust was too thin to support itself once the mobile interior flowed away, and collapsed, forming the depression. The resulting collapse pit is lined with broken fragments of lava crust. Two collapse depressions occur on the upper flanks of the cone (Figs. 3 and 5). One is an oval measuring 70 by 30 m, and the other is circular and 35 m in diameter. A 10 m wide and 45 m long shallow trough connects the two depressions.

Two hundred and thirty meters downslope from the collapse pits is a well-defined *rootless shield* (unit rs on Fig. 3; also see Fig. 6). As observed in lava flows in Hawaii, a rootless shield is formed by a tumulus on the flow surface that lifts the semi-hardened crust into a dome that rises above the surrounding flow (Patrick and Orr, 2012). Fractures in the domed crust allows interior lava to escape and flow away in all directions forming a radial pattern of lava channels. Rootless shields at Aden rise a few meters above the surface. Their central pits range from 3 to 10 meters in diameter and 1 to 3 m deep. Rootless shields are found at several places in the scabby flow facies (Fig. 3).

Six *blocky rimmed pits* are the largest of the pits on the flanks of the cone (unit br on Fig. 3). They generally range from 60 m to 250 m across, and the largest is elongate and 330 by 60 m across (Fig. 7). All blocky rimmed pits are located on the scabby flow unit. They are irregularly shaped in plan view and are surrounded by a raised rim of broken, blocky basalt (Fig. 6). The floor material on the interior is relatively smooth, and cut by large, intersecting fractures. The floor is approximately the same elevation as the flow surface outside the rims. The broken blocky rims exhibit a double crest with an intervening trough that occupies a similar position as the peripheral fractures observed on typical inflation plateaus (Fig. 4). Blocky rim materials overlie both smooth floor material and floor fractures (Fig. 8).

In much the same pattern as the rootless shields, lava channels are found draining away from the pit margins. Previously interpreted as explosion pits based on the presence of blocky raised rims (De Hon, 1965b; Hoffer, 1975b), these irregularly shaped pits are reinterpreted here as collapsed lava-rise tumuli (small inflation plateaus), which spilled lava to the surface at breakouts along their margins. Thus, the inflated flow surface of the plateau sank back to near-previous flow-surface level as lava spilled out of the interior. The blocky raised rims are simply fractured remnants of lava crust at the margins of the feature that could not support the incipient plateau after removal of the underlying lava (Fig. 9). It is also noted that the irregular shape of the rims of these features in plan view (Figs. 6 and 7) is inconsistent with the interpretation that they formed as explosion craters.

A blocky rimmed pit in an early stage of development is preserved near the terminus of the scabby flows (Fig. 7). Here, a partially collapsed inflation plateau displays a typical, steep, inflated flow front on its northwestern flank, but has collapsed on its southeastern margin. Hence, the originally horizontal, raised plateau surface is tilted and slopes to the southeast to terminate at a double-crested, blocky rim.

Discussion and conclusions

We identify five volcanic facies (Fig. 3, units cr, ch, lo, sc and if) on the Aden shield volcano based on surface physiography. The crater facies (unit cr) consist of several physiographic features including the spatter rim, lava lake basalts, rim fissures, spatter cone, inner crater, and fumaroles. The conical summit of the shield consists of channeled and lobate flow facies (units ch and lo), which are built on antecedent, thin, scabby lavas (unit sc). The flow field beyond the cone consists of thin scabby flows and thicker, inflated basalt flows (unit if). Age relations between the flow facies beyond the cone are not always clear, but in general, the scabby flows are the oldest flows on which the cone is built. The scabby flows near the cone exhibit failed attempts at inflation while the lava crust was still weak. This phase is marked by the rootless shields and blocky rimmed depressions. As the crust thickened tumuli and inflation plateaus developed in the distal flow field.

Pits on the flanks of the Aden cone are a continuum of landforms generated by similar processes as governed by the rheology of the lavas. Simple collapse pits form by collapse of thin, weak lava crust over voids created by removal of lava beneath the crust. Rootless shields

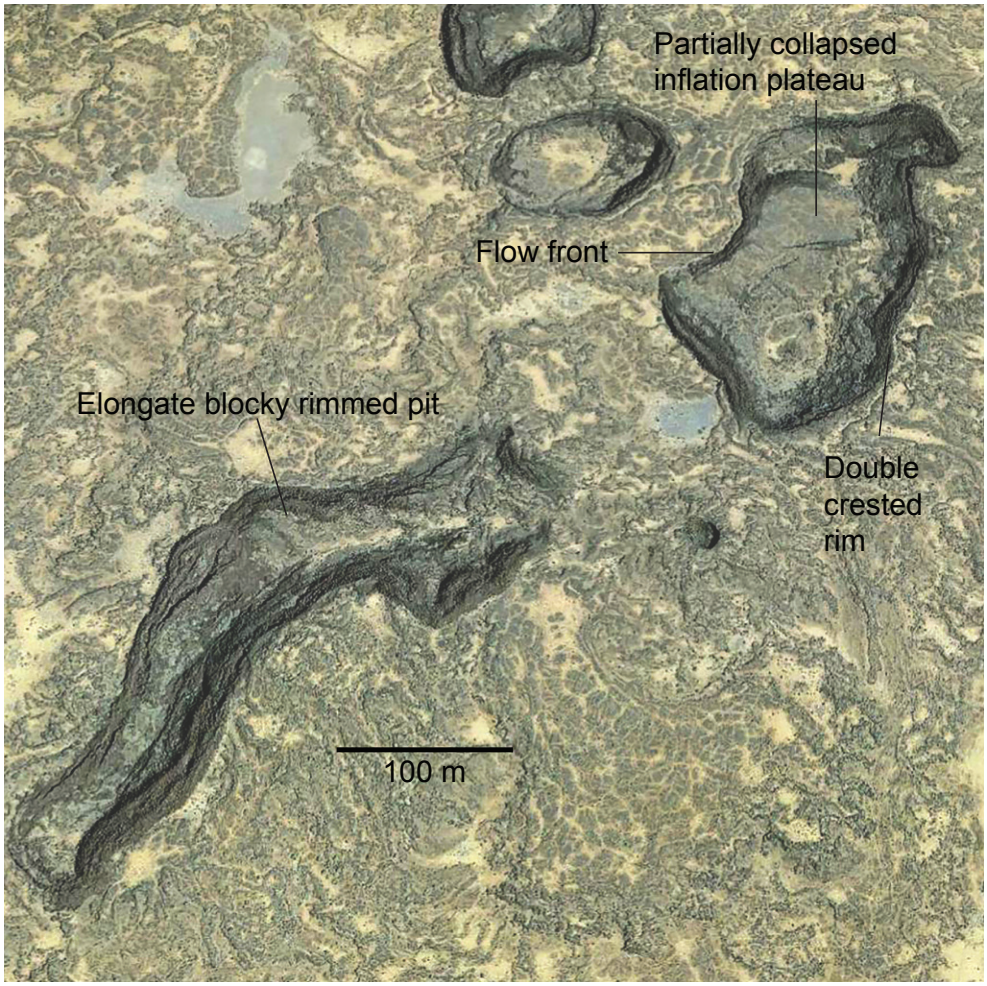

Figure 7. Aerial photograph of an elongate blocky rimmed pit and a partially collapsed inflation plateau (approximately 2 km E-NE of the Aden crater in Fig. 3) near the northern end of the scabby flow facies. The partially collapsed plateau exhibits features of both inflation plateaus and blocky rimmed pits. It is flanked on the west by a steep, blocky flow front, and on the east by a double-crested blocky rim. The interior is a comparatively smooth surface that slopes from the raised flow front to the raised blocky rim.

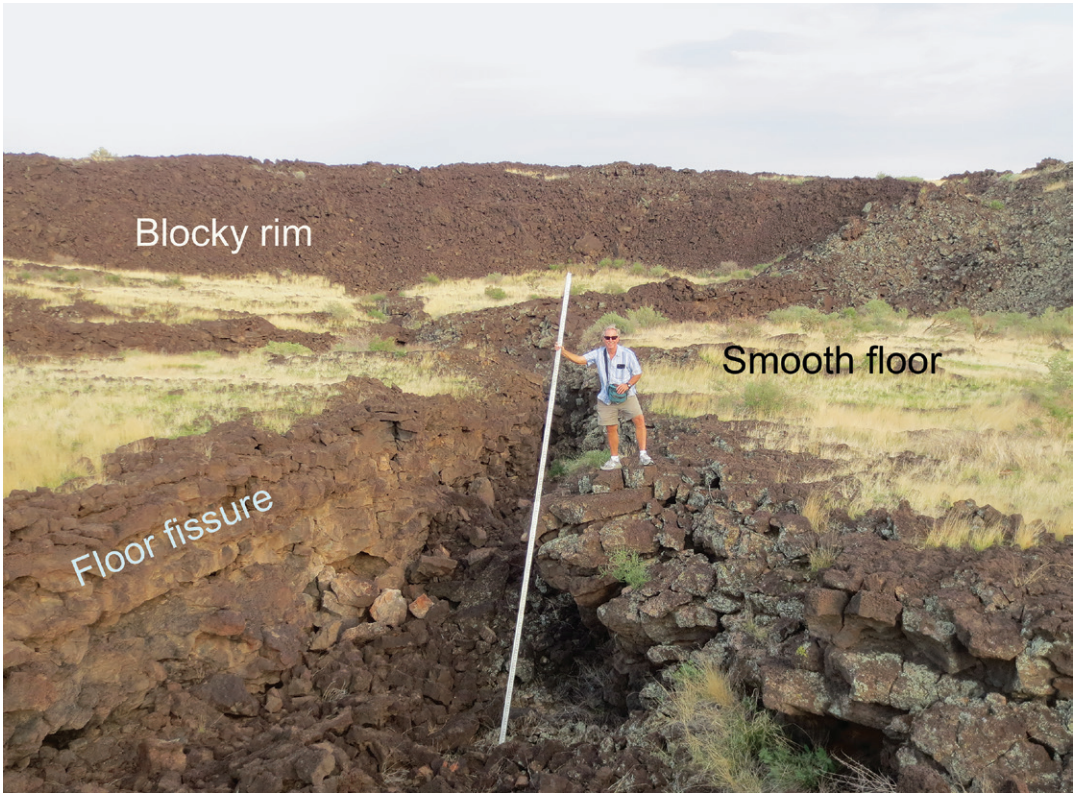

Figure 8. Photograph of a fissure on the floor of a blocky rimmed pit. The blocky rim material in the background overlies both the floor and the fissure. The blocky rim formed as solidified crust was stretched and broken during collapse of the incipient plateau surface.

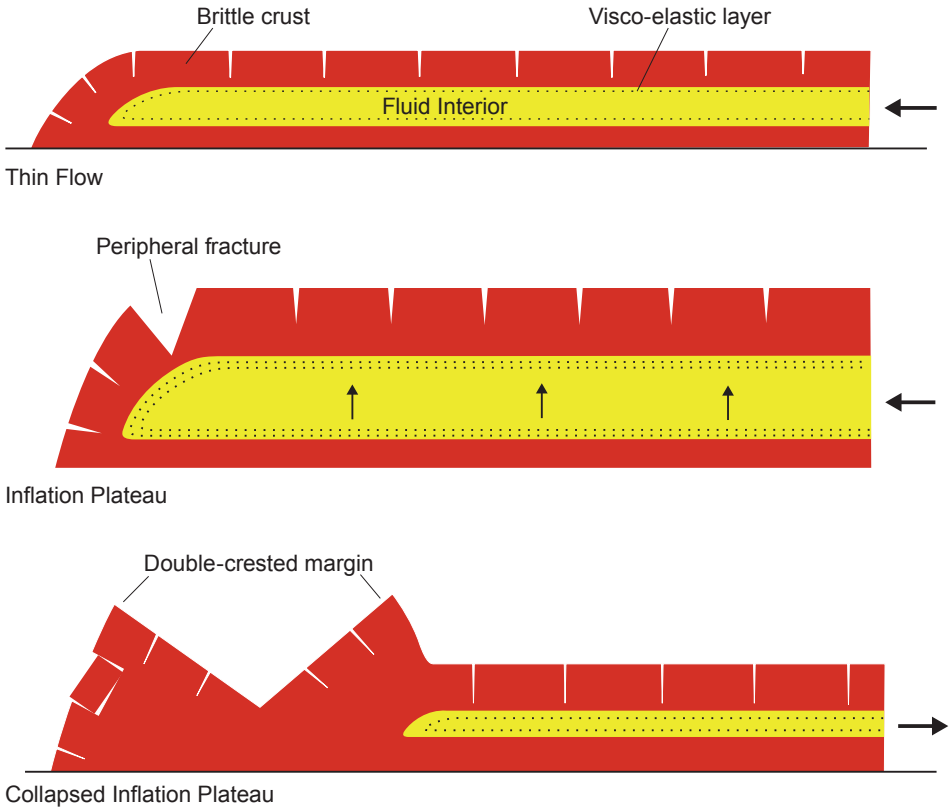

Figure 9. Cartoon of the formation of blocky rimmed pits. *Thin Flows* have a thin crust, an intermediate ductile layer, and a fluid interior. *Inflation Plateaus* form as the crust thickens, spreading is impeded, and internal pressure lifts the crust. Inflation plateaus exhibit deep fissures outlining the outer edge, and extensional jointing in the stretched upper surface. *Collapsed Plateaus* form when breakouts along the flow margins remove internal fluid lavas, allowing the plateau surface to sag back to pre-inflation levels. Brecciated lava crust forms a double-crested, blocky rim around the sunken interior.

form as crust strengthens and is pushed up into small tumuli on the surface of the flow. Breakouts of lava from the tumuli form radial lava channels. As stronger crusts develop, tumuli form small, flat-topped inflation plateaus. At some early formed plateaus, lava breakouts around the periphery cause the plateau to deflate and form blocky-rimmed depressions. Finally, lava crusts develop sufficient strength to retain lava infusions and to inflate to form large, high-standing lava plateaus. Inflation pits formed where lava inflated around subjacent rises in the pre-flow surface.

The alignment of pits on the south flank of the cone were previously assumed to be evidence of the trace of faults beneath the lava flows that served as conduits for eruptions to the surface (De Hon, 1965b; Hoffer, 1975b). The southeast trend of the pits was thought to be evidence of venting along the hypothetical Aden fault (Hoffer, 1976a). East of the cone, an apparent northeast trend of pits was thought to be evidence of venting along the Robledo fault trend. Our current analysis does not require active volcanic venting at the sites of the pits. Indeed, the pits are explained by processes that commonly occur within actively flowing lava.

The earliest flows from the Aden vent were controlled by existing topography, and spread eastward and in a narrow stream southward. As the flows spread away from the source their surface crust thickened, breached tumuli formed rootless shields and failed inflation plateaus (blocky-rimmed depressions). As these flows developed a more resistant surface crust they were able to build increasingly more substantial inflation plateaus, and ultimately accumulations of slightly more viscous lavas built the Aden cone.

Acknowledgments

The authors are indebted to James Zimmerman and unnamed reviewers for their comments and suggestions for improvement of the manuscript. Jeanett Bosarge, graduate assistant, helped with the graphics.

References

Anthony, E.Y., and Poths J., 1992, ^{3}He surface exposure dating and its implications for magma evolution in the Potrillo volcanic field, Rio Grande Rift, New Mexico, USA: Geochimica et Cosmochimica Acta, v. 56, p. 4105–4108.

Barbante, C., Fischer, H., and Wolff, E.W., 2010, Climate of the last million years: New insights from EPICA and other records: Quaternary Science Reviews, v. 29, p. 1–7.

Bersch, M.G., 1977, Petrology and geology of the southern West Potrillo basalt field, Doña Ana County, New Mexico [MS thesis]: El Paso, University of Texas at El Paso, 59 p.

Betancourt, J.L., Rylander, K.A., Penalba, C., and McVickar, J.L., 2001, Late Quaternary vegetation history of Rough Canyon, south-central New Mexico, USA: Palaeogeography, Palaeoclimatology, Palaeoecology, v. 165, p. 71–95.

Bulloch, H.E., Jr., and Neher, R.E., 1980, Soil survey of Doña Ana County area, New Mexico: Washington, DC, U.S. Department of Agriculture, Soil Conservation Service, 177 p.

De Hon, R.A., 1965a, Maare of La Mesa: New Mexico Geological Society, Guidebook 16, p. 204–209.

De Hon, R.A., 1965b, The Aden Crater lava cone: Compass, v. 43, p. 34–40.

Hawley, J.W., 1981, Pleistocene and Pliocene history of the International Boundary area, southern New Mexico; *in* Hoffer, J.M., and Hoffer, R.L., eds., Geology of the Border, southern New Mexico and northern Chihuahua: El Paso Geological Society, 1981 Field Trip Guidebook, p. 26–32.

Hoffer, J.M., 1971, Herradura: a new lava flow feature: Geological Society of America Bulletin, v. 82, p. 2949–2954.

Hoffer, J.M., 1975a, A note on the volcanic features of the Aden Crater area, southcentral New Mexico: New Mexico Geological Society, Guidebook 26, p. 131–134.

Hoffer, J.M., 1975b, The Aden-Afton basalt, Potrillo volcanics, south central New Mexico: Texas Journal of Science, v. 26, p. 379–390.

Hoffer, J.M., 1976a, Geology of the Potrillo basalt field, south-central New Mexico: New Mexico Bureau of Mines and Mineral Resources, Circular 149, 30 p.

Hoffer, J.M., 1976b, The Potrillo basalt field, south-central New Mexico: New Mexico Geological Society, Special Publication 5, p. 89–92.

Hoffer, J.M. (ed.), 1990, Geological excursions in the El Paso area: Volume 1—Aden Crater and vicinity: El Paso Geological Society 1990 Field Trip Guidebook, 42 p.

Hoffer, J.M., 2001, Geology of Potrillo Maar, southern New Mexico and northern Chihuahua, Mexico: New Mexico Museum of Natural History and Science, Bulletin 18, p. 137–140.

Hon, K.J., Kauahikaua, R., Denlinger, J., and MacKay, K., 1994, Emplacement and inflation of pahoehoe sheet flows: observations and measurements of active lava flows on Kīlauea Volcano, Hawaii: Geological Society of America Bulletin, v. 106, p. 351–370.

Kahn, P.A., 1987, Geology of Aden Crater, Doña Ana County, New Mexico, [MS thesis]: El Paso, University of Texas at El Paso, 89 p.

Keszthelyi, L., Thordarson, T., McEwen A., Haack H., Guilbaud M., Self S., and Ross, M., 2004, Icelandic analogs to Martian flood lavas: Geochemistry, Geophysics, Geosystems, v. 5, Q11014, doi:10.1029/2004GC000758.

Kilburn, J.E., Stoeser, D.B., Zimbelman, D.R., Hanna, W.F., and Gese, D.D., 1988, Mineral resources of the West Potrillo Mountains-Mount Riley and the Aden Lava Flow Wilderness Study Areas, Dona Ana and Luna Counties, New Mexico: U.S. Geological Survey, Bulletin 1735, 14 p.

Lull, S., 1929, A remarkable ground sloth: Memoirs of the Peabody Museum of Yale University, v. 3, p. 1–39.

Mack, G.H., Seager, W.R., Leeder, M.R., Perez-Arlucea, M., and Salyards, S.L., 2006, Pliocene and Quaternary history of the Rio Grande, the axial river of the southern Rio Grande Rift, New Mexico, USA: Earth-Science Reviews, v. 79, p.141–162.

Padovani, E.R., and Reid, M.R., 1989, Field guide to Kilbourne Hole maar: New Mexico Bureau of Mines and Mineral Resources, Memoir 46, p. 174–185.

Page, R.O., 1975, Malpais maar volcano: New Mexico Geological Society, Guidebook 28, p. 135–137.

Patrick, M.R. and Orr, T.R., 2012, Rootless shield and perched lava pond collapses at Kīlauea Volcano, Hawai'i: Bulletin of Volcanology, v. 74, p. 67–78.

Perkins A.M., 1949, South-central New Mexico's sink-holes and craters: Earth Science Digest, v. 4, no. 5, p. 3–11.

Reeves, C.C., Jr., and De Hon, R.A., 1965, Geology of Potrillo Maar, New Mexico and Chihuahua, Mexico: American Journal of Science, v. 263, p. 401–409.

Scheidt, S.P., Hamilton, C.W., Zimbelman, J.R., Bleacher, J.E., Garry, W.B., de Wet, A.P., and Crumpler, L.S., 2014, Lava-rise plateaus and inflation pits within the McCartys flow, New Mexico, USA: 45th Lunar and Planetary Science Conference, The Woodlands, TX, Abstract 1491.

Seager, W.R., Hawley, J.W., Kottlowski, F.E., and Kelley, S.A., 1987, Geologic map of east half of Las Cruces and northeast El Paso 1° x 2° sheets, New Mexico: New Mexico Bureau of Mines and Mineral Resources, Geologic Map 57, scale: 1:125,000.

Seager, W.R. and Mack, G.H., 1994, Geology of East Potrillo Mountains and vicinity, Doña Ana County, New Mexico: New Mexico Bureau of Mines and Mineral Resources, Bulletin 113, 27 p.

Seager, W.R., and Morgan, P., 1979, Rio Grande rift in southern New Mexico, west Texas, and northern Chihuahua; *in* Riecker, R.E. (ed.), Rio Grande rift: tectonics and magmatism: Washington, D.C., American Geophysical Union, p. 87–106.

Seager, W.R., Shafiqullah M., Hawley, J.W, and Marvin, R.F., 1984, New K-Ar dates from basalts and evolution of of the southern Rio Grande Rift: Geological Society of America Bulletin, v. 95, p. 87–99.

Self, S., Keszthelyi, L., and Thordaron, T., 1998, The importance of Pāhoehoe: Annual Review of Earth and Planetary Sciences, v. 26, p. 81–110.

Simons, E.L., and Alexander, N.L., 1964, Age of the Shasta ground sloth from Aden Crater, New Mexico: American Antiquity, v. 29, p. 390–391.

Thompson, R.N., Ottley, C.J., Smith, P.M., Pearson, D.G., Dickin, A.P., Morrison, M.A., and Gibson, S.A., 2005, Source of the Quaternary alkalic basalts, picrites and basanites of the Potrillo Volcanic Field, New Mexico, USA: lithosphere or convecting mantle?: Journal of Petrology, v. 46, p. 1603–1643.

Walker, G.P.L., 1991, Structure and origin by injection of lava under surface crust, of tumuli, "lava rises", "lava-rise pits", and lava-inflation clefts" in Hawaii: Bulletin of Volcanology, v. 53, p. 546–558.

Walker, G.P.L., 2009, The endogenous growth of pahoehoe lava lobes and morphology of lava-rise edges, *in* Thordarson, T., Self, S., Larsen, G., Rowland, S.K. and Hoskuldsson, A., eds., Studies in Volcanology: the Legacy of George Walker: Special Publications of the International Association of Volcanology and Chemistry of the Earth's Interior, v. 2, p. 17–32, Geological Society, London.

Wentworth, C.K. and Macdonald, G.A., 1953, Structures and forms of the basaltic rocks in Hawaii: U.S. Geological Survey, Bulletin 994, 98 p.

Williams, W.J.W. and Poths, J., 1994, The Potrillo volcanic field, southern Rio Grande Rift; ^{3}He surface exposure dates and petrogenetic considerations [abstract]: New Mexico Geology, v. 16, p. 81.

Zimbelman, J.R., Gary, W.B., Bleacher, J.E., and Crumpler, L.S., 2011, Inflation features on distal pahoehoe portion of the 1859 Mauna Loa Flow, Hawaii: implications for evaluating planetary lava flows: 42nd Lunar and Planetary Science Conference, The Woodlands, TX, Abstract 2443.

New Mexico graduate student abstracts

New Mexico Geology recognizes the important research of graduate students working in M.S. and Ph.D. programs. The following abstracts are from M.S. theses and Ph.D. dissertations completed in the last 12 months that pertain to the geology of New Mexico and neighboring states.

New Mexico Institute of Mining and Technology

GEOCHEMISTRY AND TRANSPORT OF URANIUM-BEARING DUST AT JACKPILE MINE, LAGUNA, NEW MEXICO

Brown, Reid Douglas, M.S.

Closed mines pose significant risks to the environment and human health. Uranium mine contamination of surface water, groundwater and soil have received moderate attention, but few studies have investigated dust transport of uranium. The latter has immediate implications for remediation efforts and environmental/human health regulators. Frequent dust storms intensify aeolian transport of uranium in arid settings. At the Jackpile Mine in Laguna Pueblo, New Mexico, 15 sets of dust traps have been installed at heights of 0.25 m, 0.5 m, 1.0 m and 1.5 m above the soil surface. Some of these traps are within the mine pit, while others are up to 4 km away; dust from these sites was collected every two months. In addition, soil samples from each site were collected and sieved into eight size classes. All samples were acid digested, and the uranium content analyzed using Inductively Coupled Plasma Mass Spectrometry. We investigate whether uranium has an affinity for a particular particle size class, with interest centered on particles small enough to be completely inhaled by humans. Results show that surface concentrations of uranium vary substantially across the landscape. Distance from the pit shows no correlation with uranium in the upper 5 cm of soil. Other factors appear to control accumulation, such as vegetation height and density and topographic relief, which are known to have a significant impact on wind speeds, soil erosion and dust deposition. Our study site has over 150 m of relief and intricate topography that lead to a range of wind speeds between sites. The soil uranium content determined at 15 sites has been compared to site elevation and vegetation height. Analysis suggests that elevation and vegetation height may impact local erosion and deposition of uranium contamination. Dust mass was collected at each height and converted into a flux (g/d/m2). The relationship between mass flux and height above ground followed a power law relationship as supported by previous research (Zingg 1953; Butterfield 1999; Dong et al 2003; Dong et al 2004a, 2004b). Particle size fractionation during aeolian transport led to an increase in metal concentrations in 4 of 6 metals of concern in the dust compared to the soil.

LITHOFACIES ANALYSIS OF THE SIERRA LADRONES FORMATION, SOUTHERN ALBUQUERQUE BASIN, N.M.: IMPLICATIONS FOR CLIFF FAULT ACTIVITY DURING THE EARLY PLEISTOCENE

Celep, Eda, M.S.

This study uses stratigraphic relations to interpret tectonic activity of the Cliff fault during the early Pleistocene. The north-striking, 60° west-dipping, ~13 km-long Cliff fault is the easternmost of three exposed Quaternary normal faults in the southwestern Albuquerque Basin of the Rio Grande rift. Previous studies have suggested that the Cliff fault was active during the late and middle Pleistocene, but early Pleistocene activity is conjectural. The other two Quaternary normal faults in the study area are the Loma Blanca and Loma Pelada faults. Comparing the long-term displacement history of the three faults allows us to determine if extensional strain has focused inward in this part of the rift, as inferred in the Española and Palomas-Winston basins of the Rio Grande rift. In addition, analyzing displacement gradients of the Cliff fault along strike allows inferences regarding fault structure and continuity of this fault to the south, where it is buried by Quaternary deposits.

The strata on the footwall of the Cliff fault are the Sierra Ladrones Formation; a Pliocene-early Pleistocene deposit composed mainly of sand with minor gravel and clay-silt. The footwall provides information on Sierra Ladrones stratigraphic units away from the potential fault related sedimentation on the immediate hanging wall of the Cliff fault. The footwall units also allow correlation of stratigraphic units between the footwall and hanging wall to obtain fault throw estimates. The footwall sediments were grouped into two different lithofacies assemblages: basin floor and distal alluvial fan. The basin floor lithofacies assemblage is subdivided into three different lithofacies; the Rio Puerco channel fill, Rio Salado channel fill and floodplain lithofacies. The alluvial fan lithofacies assemblage is very minor and consists of hyper-concentrated flow deposits from the Rio Salado drainage. In addition to these lithofacies assemblages, eolian lithofacies and some paleosols were observed with Stage I to II calcium carbonate accumulation.

The hanging wall strata are studied to find direct evidence of fault-related angular unconformities, upward splaying of stratal tilts, or fault scarp colluvium, or indirect evidence relate to sedimentation patterns. The hanging-wall strata are well-exposed in three topographic bowls. The strata consist of stream-flow gravels, that are clast supported and imbricated, and hyper-concentrated flow deposits on the toe of the Rio Salado alluvial fan, fault scarp colluvium, and playa deposits. In addition, there are paleosols with Stage-II and Stage-III calcium carbonate accumulation. Six layer-cake stratal units on the hanging wall are recognized. These range from 3 m to 30 m thickness and are called Hanging wall-1 to Hanging wall-6 (oldest to youngest). In the southernmost part of the study area, in Hanging wall-1, cemented conglomerate stratigraphy is similar to footwall Rio Salado channel fill. This gives a minimum throw of 46 m for that part of the fault.

Only the Hanging wall-6 sediment package was studied in detail to assess evidence for syn-depositional fault displacement. Eleven lithostratigraphic units were recognized

in the Hanging wall-6 layer-cake unit. These subunits are (listed from bottom to top): the lower gray subunit (Qslg), lower red sediment (Qslr), well-sorted sand (Qsws), lower brown sediment (Qslb), upper red sediment (Qsur), copper-colored gravelly sand sediment (Qsc), gray gravel sediment (Qsgg), upper brown sediment (Qsub), double soil (Qsds), tan sediment (Qst), and upper gray gravel sediment (Qsug). Inferred paleodepositional environments for the Hanging wall-6 sediment package includes playa, intra-fan depositional lobes (some oriented parallel to the Cliff fault), fault scarp colluvium and slope wash sediments.

There are indications for early Pleistocene movement of the Cliff fault in the Hanging wall-6 layer-cake unit. These include local upward splaying of stratal tilts, lateral facies variations and paleoflow parallel to the fault, thickness changes, local lateral coarsening trends towards the fault, and fault scarp colluvium. An abrupt upward splaying of stratal tilts (from 5° to 2° degrees), occurring across a 3 m thick wedge-shaped, internally massive unit, is present in the middle bowl. The presence of fan deposits transitioning south-to-north into playa deposits suggests a topographic obstruction on the east-sloping Rio Salado fan, consistent with a fault scarp. In the middle topographic bowl, pebbly to clayey sand of the copper unit and the double soil unit thicken towards the fault and pinch out towards the west. The upper brown unit in the northern topographic bowl -composed of clay, silt, and sand (inferred playa facies)- becomes coarser towards the fault. The uppermost two units, interpreted to be scarp-abutment fans elongated parallel to the fault scarp, exhibit southwest paleoflow. These two units also thin and become finer-grained to the south. The copper-colored and lower alluvial fan units interfinger with interpreted fault scarp colluvium and slope wash sediments. Colluvium sediments include cemented conglomerates and pebbles with calcium carbonate accumulation on their surface - interpreted to be reworked from the footwall. These observations provide evidence for early Pleistocene activity of the Cliff fault.

The hanging wall lithofacies assemblages differ from footwall lithofacies assemblages. Very short-distance fault-scarp derived debris and slope-wash sediments are observed. They interfinger with sediments that were carried by small fan and alluvial fan drainages. These sediments consist of playa and sand mixed sediments. The paleoflow and deposition history of alluvial –playa sedimentation on the hanging wall provides evidence for fault activity because the hanging wall preserves deposits from fault-deflected drainages (scarp abutment fans). Paleoflow data show that the paleoflow history starts with easterly- southeasterly directed small-fan, mixed-sand deposits and playa muds. Then, small fan drainages flow to the northeast. Next, flow is toward the southwest; these drainages were deflected by the fault scarp. In addition, at least six soils were developed on the hanging wall, implying that the landscape was stable between periods of deposition. There was fault activity during and between depositions of some of the units.

The results of this study have two implications of general interest. The paleoseismic history of faulting in the study area suggests that there is inward progression of extensional deformation; faults become younger towards a gravity low and corresponding syncline axis, inferred to be the depocenter of the southernmost Albuquerque basin. Inward progression occurs because the Silver Creek fault became inactive prior to the Quaternary; there is no clear trend of the Loma Pelada, Loma Blanca, and Cliff faults. Second, elevation vs. distance graphs of various lithologic contacts indicates a southward-decreasing displacement gradient of the Cliff fault. This implies two structural scenarios: 1) the Cliff fault in the study area and what was called the Cliff fault in the San Acacia area (to the south) may be linked by a relay ramp, or 2) the Cliff fault does not continue to the San Acacia area as an effectively linked structure, as was interpreted by previous workers.

DEEP RESISTIVITY IMAGING OF THE CENTRAL RIO GRANDE RIFT USING 3-D INVERSE MODELS OF MAGNETOTELLURIC DATA, WITH IMPLICATIONS FOR HYDROLOGIC AND GEOTHERMAL PROCESSES

Folsom, Matthew T., M.S.

A 3-D electrical resistivity model of the central Rio Grande rift, centered over ground surface deformation attributed to the Socorro magma body, has been generated using magnetotelluric data from 17 stations. Resistivity models were constructed using 2-D and 3-D inversion techniques, and results from the different approaches are compared and evaluated. The survey has close station spacing (~ 2 km) along a single east-west transect, but is sparsely populated with data elsewhere in the domain. A surprising result is that the zone of ground surface uplift is found to lie directly over a resistive body (~1600 Ω m) that rises to shallow depths under the Lemitar Mountains and potentially extends greater than 15 km in depth. The shallowest portion of this body lies under and to the south of the center of uplift. The Socorro Basin is found to contain a lens of low-resistivity basinal brines (0.3 – 0.5 Ω m) between 800 m and 1400 m depth, within the lower Santa Fe Group, and compartmentalized between the Loma Pelada Fault and mid-basin Cliff Fault. These structures may play a role in moving quantities of these brines upwards, where they mix with surface waters. Above the lens, the upper 800 m supports fertile agricultural lands with resistivity values ~ 10 Ω m. Although poorly constrained, low-resistivity zones (~ 90 Ω m) persists to mid-crustal depths (~ 30 km) below the Southern Albuquerque Basin and the town of Socorro. 3-D forward modeling is used to explain how 2-D inverse methods can generate spurious conductors at depths > 20 km. The phenomena can be explained solely by complex 3-D geometry of sedimentary basins in the upper 4 km of the Earth's crust.

^{40}AR/^{39}AR DETRITAL SANIDINE DATING OF THE OGALLALA FORMATION, LLANO ESTACADO, SOUTHEASTERN NEW MEXICO AND WEST TEXAS

Henry, Kevin D., M.S.

This study utilizes high precision ^{40}Ar/^{39}Ar geochronology of detrital sanidine (DS) to determine the sedimentary provenance and maximum deposition age for the Ogallala Formation. More than 1000 K-feldspars were dated from 14 samples, which define 4 unique age distributions that correlate

to location. The maximum depositional age (MDA) for the Ogallala of the western Llano Estacado of SE New Mexico is 11.44±0.03 Ma and is time equivalent to the upper Couch Formation of the Ogallala Group in Texas. In Yellow House Canyon near Lubbock, TX the Bridwell Formation of the Ogallala Group has a MDA of 6.74±0.02 Ma consistent with the Hemphillian biostratigraphy. In eastern NM, units mapped as Ogallala yielded Pleistocene DS grains, thereby indicating inaccurate mapping. These units are likely part of the Blackwater Draw Formation. The Taiban Mesa had poor sanidine yield and the dated K-feldspars are dominated by Precambrian ages. However, a single DS grain of 8 Ma indicates late Miocene or younger deposition. Most Eocene-Oligocene detrital sanidine grains in the Ogallala are sourced from the Mogollon-Datil volcanic field with a possible minor component from the Trans-Pecos and Sierra Madre Occidental volcanic fields. Mogollon-Datil material likely comes from a Whiter River Group-equivalent rock that has been completely eroded and reworked into the Ogallala. Older DS grains are sourced from reworked underlying Mesozoic strata and if the MDA approximates the deposition age the erosion of these strata occurred prior to ~11.5 Ma in the western Llano Estacado region. The Eocene-Oligocene DS grains yield distinct populations however 65–80 Ma grains cannot be directly correlated to a known volcanic source. These could have been derived from NM and Texas Upper Cretaceous or younger strata or have been eroded from volcanic rocks associated with Laramide Orogeny volcanism in northern Mexico/southern NM. Despite the overall lack of DS grains derived from the Trans-Pecos volcanic field the current data cannot support or rule out a north-flowing ancestral Pecos river during Ogallala deposition.

SOIL EROSION RATES IN THE EVOLUTION OF A FIRST-ORDER CATCHMENT IN CENTRAL NEW MEXICO: INSIGHTS FROM RUNOFF PLOTS AND MEASUREMENT OF DUAL COSMOGENIC NUCLIDES

Ramirez Torres, Carlos Fernando, M.S.

This work is part of a collaborative research on the hillslope aspect influence on the evolution of a drainage basin. It uses both insights from runoff plots and, measurements of a dual cosmogenic nuclides approach, using ^{10}Be and ^{36}Cl, to assess geomorphic histories and the erosional rates differences between the surface of two contrasting vegetated opposite north and south-facing hillslope in Central New Mexico. Apparent cosmogenic nuclide erosion rates of 6 to 21 mm kyr^{-1} were measured with differences between aspect-oriented slopes as high as 33%; evidencing the feedback relationship of aspect and plant coverage on erosion as the more vegetated/moist north-facing slope was more resource conserving than the south-facing slope. Furthermore, the study found that our initial working hypothesis of headward erosion of the trunk drainage was not supported, as the nuclide data indicates downward incision of the entire drainage. In addition an average surface exposure age of 580 ka was obtained for the surface into which our first-order basin was incised and an age range of 60 to 180 ka was indicated as a constraint on the establishment of the current aspect-dependent erosion pattern.

EVAPOTRANSPIRATION IN MOUNTAIN TERRAIN – APPLYING TOPOGRAPHIC-BASED ENERGY CONSTRAINTS TO EVALUATE THE DISTRIBUTION OF WATER FLUXES AND EFFECT OF VEGETATION COVER CHANGE

ReVelle, Peter M., M.S.

Increasing water demands and groundwater pumping rates in semiarid regions have focused attention on improving the understanding of regional water resources and characterizing hydrological processes and quantifying their associated fluxes that ultimately determine short and long-term water supplies. The Sacramento Mountains in southeast New Mexico are a significant source of groundwater recharge for the surrounding Roswell Artesian Basin, Tularosa Basin, and Salt Basin aquifers. Land and forest management officials are interested in understanding the effects of manipulating environmental conditions, through land cover changes and forest management practices, on mountain recharge. This recharge ultimately provides much of the water supply for high water-use areas in surrounding basins. Previous work under the Sacramento Mountains watershed study has investigated various components of the water balance, including the relationship between soil water sources and tall forest vegetation, as well as quantifying runoff and canopy interception. One of the largest, most variable, and most important processes controlling mountain groundwater recharge is the total amount of water that evaporates from the soil surface or through vegetation (evapotranspiration). The focus of the present study is to examine experimental plots that have been thinned, and similar control plots that were not thinned, in order to quantify the amount of water lost to the atmosphere through evapotranspiration, in order to improve estimates of the change in the water-balance and the resulting change in groundwater recharge.

Using the remote-sensing algorithm Mapping EvapoTranspiration at high-Resolution with Internal Calibration (METRIC), satellite imagery from Landsat 5 was analyzed to estimate evapotranspiration (ET) for watershed plots for images chosen before and after thinning of the plot areas. Through solving the surface energy balance, METRIC provides spatially distributed ET estimates at 30 meter by 30 meter resolution that account for both soil and vegetation contributions to the amount of water lost as ET. We employed an environmental-impact-type analysis to compare ET estimates from METRIC before and after thinning and quantify the net impact on ET. We used linear regression to evaluate the relationship between changes in canopy cover due to vegetation removal and resulting effects on ET for thinned plots. Additional analyses used multiple linear regression to determine which surface parameters were most important in explaining the variability of the response in ET before and after thinning at the plot scale. Much larger samples across the whole Landsat image extent were also analyzed to examine large-scale distributions and identify patterns and shifts in significance of predictor variables between images. Forest-group types and land-cover classes were examined further by comparing mean ET values using a multi-comparison test that grouped statistically similar ET distributions together. This approach was taken as a way to investigate the ability of METRIC to

identify and separate individual class or group types from one another or combine similar land cover types into groups, given that specific forest group types are not supplied to METRIC. Statistical analysis of ETrF (fraction of reference ET) and associated ET values for the paired plots extracted from maps produced using METRIC show no statistically significant difference in ET (alpha = 0.10) between thinned and respective control plots between pre-thinning images, while indicating significant but variable decreases in ET between images from before and after thinning dates. The net changes in ET determined using a Before-After Control-Impact (BACI) analysis show a net decrease for all thinned plots at a 90% confidence level. Linear regression was applied to determine the relationship between the net changes in ET to the associated changes in canopy cover, showing a good fit with an R-squared value of 0.79. Additional data points were compared from a similar study in a semi-arid upland pine forest using values of canopy cover reduction and the associated effect on ET that showed close agreement to the regression line determined from the present study within a few percent. While thinning extent appears to be the primary control on the effect on ET, multiple linear regression analysis indicates that topography has an important influence on the variability of the magnitude of the effect. Changes in albedo after thinning is also an important contributing factor identified from the multiple regression analysis. The significance of albedo can be related to the physical effect of decreases in canopy cover associated with thinning treatment modifying the surface albedo and resulting net short-wave radiation for thinned plots. Large-scale analysis of ETrF estimates across the entire Landsat image provide evidence for the consistency between ETrF values from METRIC for different image dates and indicate the ability to distinguish forest groups and land cover classes through statistically significant differences in mean ETrF. The results of the ANOVA GLM analysis exhibit the same primary factors contributing to the variability in ETrF, highlighting the consistent and robust nature of METRIC derived ETrF estimates. The range of ETrF values for forest groups are reasonable and compare well with crop coefficients (ETrF) found in the literature. Multiple comparison testing between forest and NLCD groups demonstrates statistically significant differences between many forest and NLCD groups that result in similar grouping between image dates. Differences in grouping between image dates are likely influenced by the effects of varying local meteorological conditions and antecedent soil moisture. The methods utilized in the present study provide a new approach to quantifying changes in ET associated with land cover management practices through remote sensing. The current work illustrates the potential for similar types of approaches. Further analysis utilizing additional images could be applied to advance the understanding of the role of surface parameters in predicting responses in ET resulting from land cover changes through identifying and investigating significant relationships within the meta-scale patterns determined by the complex processes governing them in highly heterogeneous terrain.

ECOLOGICAL DISTURBANCES AND THE WATER BALANCE
HYDROLOGIC SCIENCES, Wine Michael, Ph.D.

As populations rise, understanding how global change impacts future water resource availability on Earth is of paramount importance. While the air temperature-water vapor pressure relationship typically plays a central role in predictions of hydrologic effects of future climate scenarios, ecological changes—including disturbances—also influence water resources. Key anthropogenic drivers of ecological change include atmospheric greenhouse gas induced global warming, long-term changes in grazing paradigms, historic fire suppression, and road construction, which have led to a widespread wildfire deficit. This wildfire deficit has caused woody encroachment and increased wildfire frequency. These modifications to wildfire regime cause a wide range of ecological and hydrologic impacts. At the low wildfire frequency end of the spectrum woody encroachment occurs, substantially reducing groundwater recharge, primarily due to longer growing season and deeper rooting depth of encroaching trees relative to grasses. At slightly higher fire frequencies fire impacts are not detectable either because they fall below a threshold value or because they are simply small in magnitude. However, in certain regions of especially high wildfire frequency, wildfires are critical generators of streamflow even at the large watershed scale, contradicting prevailing conceptual models. In such regions, wildfires create infrequent large impacts at small scales, whereas at larger scales a patchwork of wildfire occurrence yields enhanced water yields that are sustained over time. Such conditions may occur in areas with anomalously high lightning frequency. When wildfire impacts are compared to predictions of climate change impacts by 2050, we show that long-term wildfire impacts can exceed climate change impacts in certain ecoregion divisions. Finally, we implement Fuh's equation—which relates wetness index to runoff coefficient by means of water retention capacity—across 474 large watersheds covering the majority of the western USA and quantify wildfire impact on long-term water yield by watershed over the western USA.

New Mexico State University

SEDIMENTOLOGY, STRATIGRAPHY, AND GEOCHRONOLOGY FROM MIDDLE–LATE EOCENE, VOLCANIC AND VOLCANICLASTIC STRATA OF THE PALM PARK FORMATION AND OREJON ANDESITE, SOUTH-CENTRAL NEW MEXICO
Creitz, Ryan Harry, M.S.

The middle Eocene marks the terminus of Laramide deformation and initiation of the volcanic-dominated phase of the Laramide orogeny in south-central New Mexico. This tectonic transition is recorded by a suite of volcanic/subvolcanic, volcaniclastic, gypsiferous, and carbonate strata that make up the Palm Park Formation and age equivalent Orejon Andesite, Cleofas Andesite, and Rubio Peak Formation. A number of studies have focused on constraining the timing and geochemistry of the late Eocene initiation of the Rio Grande rift in southern New Mexico, yet little is known about the eruptive and depositional history just after the end of Laramide deformation and prior to the onset of rifting. Presented here are new sedimentologic, stratigraphic, geochronologic,

and provenance data from the Palm Park Formation and Orejon Andesite near Las Cruces, New Mexico.

The base of the Palm Park is marked by a progressive (erosional) unconformity with basement rocks that range in age from Paleoproterozoic–Paleocene. Basal strata consist of pebble–cobble volcaniclastic conglomerate with limestone clasts. Conglomerate units are interbedded with fossiliferous micritic limestone and gypsum-bearing strata. This lower stratigraphic interval is interpreted to represent shallow lake sedimentation and episodic lahar flows. Adjacent to a volcanic vent, proximal facies of the Palm Park consist of primarily volcanic deposits of intermediate composition that are interbedded with massive pebble–boulder volcaniclastic conglomerate with an average unit thickness >5.0 meters. These rocks are interpreted to represent lava flows and lahar debris flows. Distal strata of the Palm Park are dominated by volcaniclastic mudstone, sandstone and granule–cobble conglomerate that range in thickness from 0.01–0.5 meters. These strata are interpreted as lahar hyperconcentrated flows, water laden sheet flows, and lahar debris flows. The Orejon Andesite does not have the same stratigraphic variation as seen in the Palm Park and consists entirely of intermediate composition lava flows, pyroclastic flows, and lahar debris flows characteristic of proximal facies.

Zircons from an ash-fall tuff near the bottom and top of the Palm Park have a U-Pb age of 45.0±0.7 and 39.6±0.5 Ma respectively, whereas intermediate composition lava flows and subvolcanic units yield ages ranging from 41.6±0.7 Ma–41.0±0.6 Ma, respectively. Zircons from intermediate composition lava flows near the middle–upper Orejon Andesite have U-Pb ages ranging from 44.0±1.5–42.8±0.5 Ma and are comparable to Palm Park ages.

U-Pb detrital zircon ages from Palm Park volcaniclastic intervals exhibit primary peaks between 41–44 Ma with secondary peaks between 1600–1800 Ma, 1350–1550 Ma, and 1000–1250 Ma. Paleoproterozoic–Cretaceous age zircons are present in nearly all samples but do not make up statistically-relevant peaks. Middle Eocene peaks are interpreted to represent detrital contributions from late-stage Laramide stratovolcanoes. Sparse Paleoproterozoic–Cretaceous detrital contributions are interpreted to reflect recycled zircons that were derived from inactive Laramide uplifts and indicate the cessation of Laramide deformation. The prevalence of middle Eocene zircons indicates a volcanic-dominated phase of orogenesis in south-central New Mexico. During this final stage of the Laramide orogeny volcaniclastic sedimentation exceeded local accommodation resulting in the infilling of paleovalleys and burial of Laramide hanging wall highlands.

VOLATILE CONTENTS AND PRE-ERUPTIVE CONDITIONS OF RHYOLITIC MAGMAS FROM THE ORGAN CALDERA, SOUTHERN NM

Lente, Jenna L., M.S.

Caldera-forming eruptions in southern New Mexico ~36 Ma created one of the most aesthetically prominent features in the region- the Organ Mountains. This project combines petrography/mineralogy, major and trace element concentrations of melt inclusions, phenocrysts and whole rocks, and volatile contents of melt inclusions to determine pre-eruptive storage conditions of the magmas of the Organ caldera. The goal is to constrain magma storage conditions of large, silicic, potentially catastrophic caldera- forming eruptions. This study geochemically examines deposits from the first and last caldera-forming eruptions from the Organ caldera, the Cueva Tuff (CT) and the Squaw Mountain Tuff (SMT). Homogeneity of major and trace elements in melt inclusions and feldspars in the CT combined with the range in H_2O contents (~2.5 to 6.5 wt. %) suggest the CT was stored in a convecting magma chamber at depths of ~4 to 9 km. Melt inclusion geochemistry indicates fractional crystallization was the dominant process of melt differentiation, and that degassing and convection caused the range of volatile contents found in the melt inclusions.

Accurate volatile contents of the SMT were not determined due to crystallized melt inclusions requiring rehomogenization, resulting in H+ diffusive loss from melt inclusions. Thus, it is not possible to constrain magma chamber depths. However, major and trace element compositions of whole rocks and gradational changes in phenocryst types and abundances suggest the SMT magma chamber was stratified.

SMT melt evolution was likely complex, including fractional crystallization and magma mixing with subsequent West Side Lavas (WSL) magmas. Injection of WSL magma possibly triggered the eruption of the SMT. This study provides insight into complex processes occurring prior to large silicic eruptions, and changes the perception of the storage conditions of the CT and SMT magmas. These eruptions did not form from one large, single, stratified magma chamber as previously suggested, but likely originated from distinctive magma chambers. Additionally, it is possible that the eruption of the SMT was larger than previously thought, and could potentially be classified as a super eruption.

USING FIELD RELATIONSHIPS AND GEOCHRONOLOGY TO EVALUATE THE FORMATION OF THE SCHOOLHOUSE MOUNTAIN CALDERA, MOGOLLON-DATIL VOLCANIC FIELD, SOUTHWEST NEW MEXICO

Swenton, Vanessa Marie, B.S.

Paleogene calderas of the Mogollon-Datil and Boot Heel volcanic fields are numerous and represent the Ignimbrite Flare-up within southwest New Mexico. These calderas were active during the episodes of dominantly felsic volcanism between ~37–23 Ma in the Mogollon Datil volcanic field (MDVF) and ~35–27 Ma in the Boot Heel volcanic field (BHVF). Eruptive activity from these calderas was relatively coeval, with ignimbrites filling the depressions of subsided calderas and extensive outflow sheets emanating away from them. The history of these calderas is marked in the stratigraphy by the characteristic tuffs, breccias, and megabreccias emplaced during the violent, catastrophic collapse.

The eruptive history of the Schoolhouse Mountain caldera (SMC) is exposed in the Burro Mountains, southwest New Mexico, within the southern MDVF.

Combined field observations and field mapping, U-Pb and $^{40}Ar/^{39}Ar$ geochronology, sanidine compositions, whole rock major and trace element geochemistry, and Sr isotope geochemistry provide insight into the evolution of the SMC and a detailed account of the caldera collapse. These techniques provide a more accurate age of caldera formation, place units of the SMC into a caldera model, correlate intracaldera units with regional outflow sheets, and provide context to these units within the MDVF, Boot Heel volcanic field, and the Ignimbrite Flare- up. The precise age of the formation of the SMC was determined by definitively associating units of the Kerr Canyon sequence with the collapse of the SMC and by dating the matrix material of the collapse breccias within it. Boulder clasts up to 30 m in length were surrounded by tuff in both the upper megabreccia and the newly identified lower megabreccia in this sequence. Sanidine crystals from matrix material of the upper megabreccia yielded a prominent $^{40}Ar/^{39}Ar$ age peak of 34.93 ± 0.01 Ma, with minor peaks at 35.3 Ma, 35.6 Ma, and 35.9 Ma. These minor peaks are interpreted as represented xenocrystic contamination from the regionally extensive 35.33 ± 0.10 Ma Kneeling Nun Tuff (McIntosh et al., 1991). Without a date from the lower megabreccia, the upper megabreccia matrix age of 33.93 Ma represents the minimum age of the formation of the SMC. Two rhyolite boulder clasts from the megabreccia yielded $^{40}Ar/^{39}Ar$ ages of 35.34 ± 0.02 Ma and 35.32 ± 0.01 Ma, both of which are coeval with the Kneeling Nun Tuff. The Kerr Canyon sequence culminates with a voluminous biotite-rich ash-flow tuff and several finer-grained ash-flow and air-fall intervals. A sandstone layer in the upper Kerr Canyon sequence is interpreted as representing a hiatus in eruptive activity and marks the contact with the overlying Mangas Creek sequence.

Sanidine compositions have aided in correlating SMC tuffs with regional ignimbrites, and provided evidence to suggest the caldera source of these tuffs. Tuffs previously collectively identified as the "Box Canyon Tuff" were interpreted as being sourced from the SMC, where the Cherokee Canyon Tuff was identified as an intracaldera tuff (McIntosh et al., 1991). McIntosh et al. (1991) used the average age of all the units to represent the age of the caldera. Sixteen samples postulated to be sourced from the SMC were analyzed via electron microprobe, including all of the "Box Canyon Tuff." All analyzed samples contained sanidine phenocrysts with ~Or65 with the exception of the McCauley Ranch Tuff and the Cherokee Canyon flow, which contained notably lower orthoclase percentages of Or43 and Or55, respectively. BaO concentrations among clasts and matrix material of the Kerr Canyon sequence, and Bell Top Formation Tuff 5 are similar to those of the Kneeling Nun Tuff.

Strontium isotope geochemistry has provided additional insight into the evolution of the SMC. There are no significant trends with whole rock initial $^{87}Sr/^{86}Sr$ over time and no overall correlation with inverse Sr among rocks of the SMC. Variations in isotope data may be a result of (1) these units being sourced from a different caldera system; (2) these units were influenced by injected magma that rejuvenated the magma system sourcing the SMC; or (3) sanidines from these rocks being chemically altered from weathering. Increased biotite phenocryst abundances in the biotite-rich tuffs of the upper Kerr Canyon sequence support the potential rejuvenation of the magma system through periodic injection of magma.

Units of the Knight Peak region, thought to be potential outflow sheets sourced from the SMC (this study) are still of unknown source. Geochronology, variations in unit thickness, and whole rock geochemistry from this study has allowed for the conclusion that the JPB Mountain tuff and units of the C-Bar Canyon sequence may possibly be sourced from the SMC. The "Kneeling Nun Tuff of Hedlund 1978" and the overlying lava flow of Malpais Hills are too young to be derived from the SMC and may be sourced from other calderas within the MDVF and/or BHVF.

University of New Mexico

A MULTI-PROXY STALAGMITE RECONSTRUCTION OF THE CLIMATE OF SOUTHWESTERN NORTH AMERICA FROM THE MIDDLE TO LATE HOLOCENE

Allen, Chrissy, M.S.

The seasonal balance of moisture has a significant effect on natural ecosystems and culture in southwestern North America (SWNA), and it thus is necessary to understand the cause of this moisture variability in order to better predict the scope of potential future changes. Studies of modern SWNA climate indicate that most of the annual moisture at this site comes from monsoonal summer precipitation and a lesser amount of Pacific winter moisture. The climate of the Holocene is of particular interest for constraining natural variability of interglacial climates prior to any anthropogenicinfluence. An overall transition to a wetter Late Holocene climate in SWNA has been established by different climate proxies, and a definable shift in climate around 4.2 ka is observed in records from various locations around the world. However, the lack of highly resolved records in SWNA limits our ability to determine the mechanisms and timing of this climate shift in this region. In this study we present a high-resolution U-Th dated speleothem record from ~6500 to ~1000 yr BP of oxygen and carbon stable isotopes, Sr and Ba trace elements, grayscale, and $^{234}U/^{238}U$ isotope ratios from two caves in southeastern New Mexico. Our data suggests the climate of the Middle Holocene was warmer and dominated by monsoonal precipitation, and the Late Holocene was cooler and experienced an increase in winter precipitation. Our record further suggests this shift occurred around 4.2 ka. High-frequency climate variability observed in SWNA during the Late Holocene has been attributed to an active ENSO/PDO system, yet this was limited by lack of direct comparison with the Middle Holocene. Spectral and wavelet analyses from this study show interdecadal and decadal variation observed in the Late Holocene that is not observed in the Middle Holocene, suggesting that strengthened ENSO/PDO activity is responsible for the increased moisture observed in SWNA during the Late Holocene by increasing winter precipitation.

OBSERVED CHANGES IN CLIMATE AND STREAMFLOW IN THE UPPER RIO GRANDE BASIN

Chavarria, Shaleene, M.S.

Observed streamflow and climate data are used to test the hypothesis that climate change is already affecting the streamflow volume derived from snow accumulation in ways consistent with climate model-based projections of 21st century streamflow. Annual and monthly changes in streamflow volume and surface climate variables on the upper Rio Grande (URG) near its headwaters in southern Colorado are assessed for water years 1958–2015. Trends in discharge are examined together with variations in snow water equivalent and surface climate variables. Results indicate that temperatures in the basin have increased significantly primarily in the winter and spring seasons, April 1 snow water equivalent has decreased by approximately 25%, and streamflow has declined in the runoff season, but small increases in precipitation have reduced the impact of declining snowpack on streamflow. Changes in the snowpack-runoff relationship are noticeable in hydrographs of mean monthly streamflow, but most apparent in the changing ratio of precipitation (rain+snow, and snow water equivalent) to streamflow and in regression statistics. The observed changes impact our ability to predict streamflow on a seasonal basis and affect long-term water management of the Rio Grande.

THE DYNAMIC GEOMORPHIC SETTING OF THE LATE PLEISTOCENE HARTLEY MAMMOTH SITE: BURIAL AND SKELETAL PRESERVATION IN A SLUMP-BLOCK DEPRESSION NEAR ABIQUIU, NEW MEXICO

Muus, Jennifer, M.S.

Near Abiquiu in northern New Mexico, the skeletal remains of two mammoths were discovered in the summer of 2014 in the near-surface deposits of a very small alluvial channel. The channel occupies a depression on the backtilted top of a Toreva slump block, a highly unusual setting for a mammoth burial. Geomorphological investigation of the site has provided insight into processes leading to burial and preservation of the remains, as well as local environmental change. Field mapping of sediment sources and LiDAR scans of the contributing slope basin and slump bench provided a map of geomorphic features and surficial geologic deposits. To better understand the geomorphic context of the mammoth remains, termed the 'Hartley Mammoth,' six soil pits from the mapped surficial geologic deposits were described in the field. Bedrock and soil samples were analyzed using x-ray fluorescence (XRF), loss on ignition (LOI), x-ray diffraction (XRD) and particle size analysis. Bone collagen from a limb fragment returned a calibrated ^{14}C age for one mammoth of about 33 ka. On the mammoth site slump bench, discontinuous bouldery footslope colluvial deposits show clay films and stage l to l+ carbonate, and were likely deposited shortly following slumping due to failure of oversteepened slump scarps. The deposit surrounding the mammoth remains consists of cobbles and small boulders of sandstone supported by a muddy matrix; this texture strongly suggests that the remains were buried by a debris flow. The debris-flow deposit created a high point in the channel, so that subsequent flow was diverted off the downslope edge of the slump block, protecting the mammoth remains from later erosion. Ped-face carbonate coatings (stage I+) in the debris-flow deposit indicate a greater age than the relatively well-sorted and stratified alluvial deposits in the channel above the debris flow. Following mammoth burial, incremental deposition of finer footslope colluvium continued to the present. Overall, field observations, XRF and XRD analyses indicate that despite the ~33 ka age of the mammoth, very little chemical weathering and limited soil development has occurred in the debris flow and other surficial deposits of apparent late Pleistocene age in this dynamic environment.

NEW MEXICO BUREAU OF GEOLOGY & MINERAL RESOURCES

Publications 2018

Order online or shop at our bookstore!

Memoir 50

Energy and Mineral Resources of New Mexico

Edited by Virginia T. McLemore, Stacy Timmons, and Maureen Wilks.

NMBGMR Memoir 50/NMGS Special Publication 13.
Six-volume boxed set $125.00.
Individually $25.00.

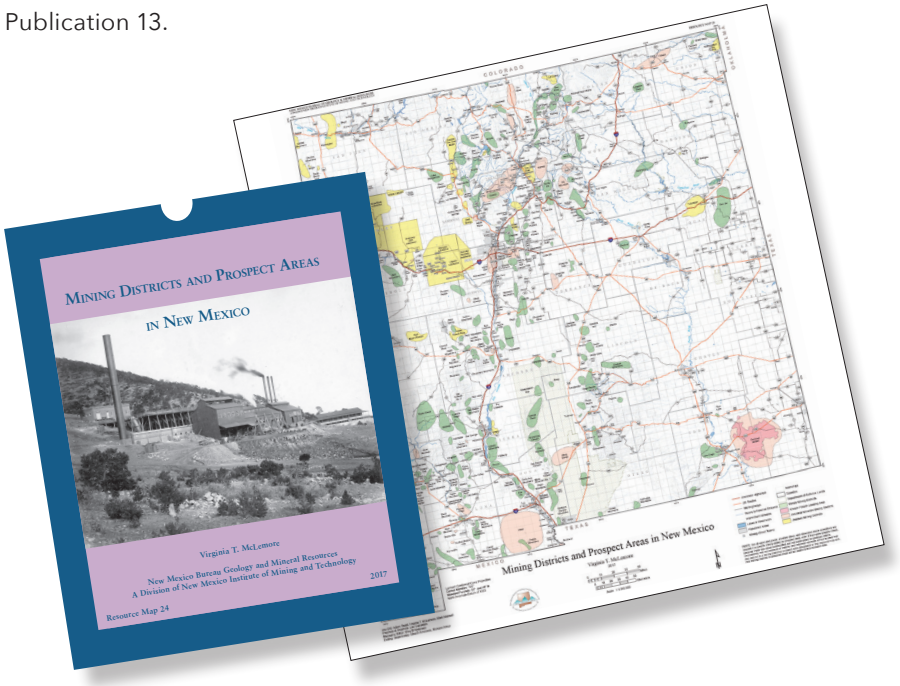

Resource Map 24

Mining Districts and Prospect Areas in New Mexico

By Virginia T. McLemore, edited by Shari Kelley.
Map, booklet, and Appendix 1;
$18.95.

For more information about the bureau and our publications:

Visit our website at **http://geoinfo.nmt.edu**
Call **(575) 835-5490**, e-mail us at **NMBG-Publications@nmt.edu**,
or visit our Bookstore at the corner of Bullock and Leroy
on the campus of New Mexico Tech
801 Leroy Place, Socorro, New Mexico, 87801

New Mexico Bureau of Geology and Mineral Resources
New Mexico Tech
Earth Science for the 21st Century

NEW MEXICO TECH
SCIENCE · ENGINEERING · RESEARCH · UNIVERSITY